Application of amine-functionalized titanium dioxide wrapped in reduced graphene oxide in photocatalytic degradation of methylene blue

Miss Sirinya Kanjanapanasont

A Thesis Submitted in Partial Fulfillment of the Requirements

for the Degree of Master of Engineering in Chemical Engineering

Department of Chemical Engineering

Faculty of Engineering

Chulalongkorn University

Academic Year 2018

การประยุกต์ใช้ไทเทเนียมไดออกไซด์ที่มีหมู่ฟังก์ชันเอมีนซึ่งหุ้มด้วยรีดิวซ์กราฟีนออกไซด์ใน
กระบวนการย่อยสลายเมทิลีนบลูที่เร่งปฏิกิริยาแบบใช้แสง

น.ส.สิรินญา กาญจนพนาสณฑ์

Thesis Title   Application of amine-functionalized titanium dioxide
                      wrapped in reduced graphene oxide in photocatalytic
                      degradation of methylene blue
By   Miss Sirinya Kanjanapanasont
Field of Study   Chemical Engineering
Thesis Advisor   Akawat Sirisuk, Ph.D.

Accepted by the Faculty of Engineering, Chulalongkorn University in Partial Fulfillment of the Requirement for the Master of Engineering

             Dean of the Faculty of Engineering
(Professor SUPOT TEACHAVORASINSKUN, D.Eng.)

THESIS COMMITTEE

             Chairman
(Professor PAISAN KITTISUPAKORN, Ph.D.)

             Thesis Advisor
(Akawat Sirisuk, Ph.D.)

             Examiner
(Associate Professor KASIDIT NOOTONG, Ph.D.)

             External Examiner
(Assistant Professor Okorn Mekasuwandumrong, D.Eng.)

สิรินญา กาญจนพนาสณฑ์ : การประยุกต์ใช้ไทเทเนียมไดออกไซด์ที่มีหมู่ฟังก์ชันเอมีน ซึ่งหุ้มด้วยรีดิวซ์กราฟีนออกไซด์ในกระบวนการย่อยสลายเมทิลีนบลูที่เร่งปฏิกิริยา แบบใช้แสง. (Application of amine-functionalized titanium dioxide wrapped in reduced graphene oxide in photocatalytic degradation of methylene blue) อ. ที่ปรึกษาหลัก : อ. ดร.อัครวัต ศิริสุข

งานวิจัยนี้ศึกษาผลของการเติมรีดิวซ์กราฟีนออกไซด์ลงในตัวเร่งปฏิกิริยาไทเทเนียม ไดออกไซด์ที่ติดหมู่ฟังก์ชันเอมีน โดยปริมาณของรีดิวซ์กราฟีนออกไซด์ที่ศึกษาอยู่ในช่วง 0 ถึง 0.05 โดยน้ำหนัก นอกจากนี้ยังศึกษาผลของปริมาณเอมีนโดยใช้ 3-อะมิโนโพรพิลไตรเมท็อกซี ไซเลน (APTMS) ในการเตรียมตัวเร่งปฏิกิริยา TiO_2/rGO ปริมาณของ APTMS ศึกษาที่ 2.21 และ 22.1 มิลลิโมล ในการสังเคราะห์ตัวเร่งปฏิกิริยาไทเทเนียมไดออกไซด์ใช้วิธีโซลเจล นำ ไทเทเนียมไดออกไซด์มาปรับปรุงพื้นผิวด้วย APTMS โดยการรีฟลักซ์ จากนั้นใส่กราฟีนออกไซด์ ลงไปเพื่อให้หุ้มไทเทเนียมไดออกไซด์ที่ติดหมู่ฟังก์ชันเอมีน และทำการรีดักชันให้เป็นรีดิวซ์ก ราฟีนออกไซด์โดยใช้ไฮดราซีนและแอมโมเนีย ในการทดลองตัวเร่งปฏิกิริยาถูกกระจายใน สารละลายเมทิลีนบลูก่อนทำการฉายแสงยูวีหรือวิสิเบิล การเพิ่มปริมาณรีดิวซ์กราฟีนออกไซด์ ในตัวเร่งปฏิกิริยา ส่งผลให้ประสิทธิภาพของตัวเร่งปฏิกิริยาในการย่อยสลายสารละลายเมทิลี นบลูสูงขึ้น โดยสัดส่วนของรีดิวซ์กราฟีนออกไซด์ที่ให้ประสิทธิภาพสูงสุดคือปริมาณรีดิวซ์ก ราฟีนออกไซด์ร้อยละ 4 โดยน้ำหนักซึ่งมีปริมาณ APTMS 2.21 มิลลิโมล ให้ค่าประสิทธิภาพ สูงสุดที่ร้อยละ 70.63 ภายใต้แสงยูวี และร้อยละ 31.06 ภายใต้แสงวิสิเบิล ผลการทดลองการ ย่อยสลายสารละลายเมทิลีนบลูโดยใช้ในตัวเร่งปฏิกิริยา TiO_2/rGO และ TiO_2/rGO^* สอดคล้อง กับผลของ PL และ UV-Vis ซึ่งการเพิ่มปริมาณรีดิวซ์กราฟีนออกไซด์ส่งผลให้ลดการกลับมา รวมกันของคู่อิเล็กตรอนและโฮล และช่วยดูดซับแสงได้ดียิ่งขึ้น อีกทั้งปริมาณ APTMS ที่ลดลง ส่งผลให้ช่องว่างระหว่างแถบพลังงานแคบลง

สาขาวิชา	วิศวกรรมเคมี	ลายมือชื่อนิสิต
		....
ปี	2561	ลายมือชื่อ อ. ที่ปรึกษาหลัก
การศึกษา		....

6070338321 : MAJOR CHEMICAL ENGINEERING

KEYWORD: Titanium dioxide, APTMS, rGO, Methylene blue, Photocatalytic degradation

Sirinya Kanjanapanasont : Application of amine-functionalized titanium dioxide wrapped in reduced graphene oxide in photocatalytic degradation of methylene blue. Advisor: Akawat Sirisuk, Ph.D.

This research investigated the effect of reduced graphene oxide (rGO) addition to amine-functionalized titanium dioxide (APTMS-TiO$_2$). The loading amount of rGO was varied from 0 to 0.05 %wt. Also, the effect of the amount of 3-aminopropyltrimethoxysilane (APTMS) was studied. To synthesize TiO$_2$/rGO catalysts, the amount of APTMS was varied at 2.21 and 22.1 mmol. TiO$_2$ catalyst was synthesized via a sol-gel method. Next, the surface of TiO$_2$ was modified with APTMS by refluxing. Then graphene oxide was wrapped around APTMS-TiO$_2$ and was reduced to rGO using hydrazine and ammonia. In the experiment, the catalyst was dispersed in methylene blue solution before being exposed to either UV or visible light. An increase in the amount of rGO in the catalyst improved photocatalytic activity for degradation of methylene blue. The amount of rGO that produced the highest conversion is 0.04% with the amount of APTMS of 2.21 mmol. Its highest efficiencies were 70.63 % under UV light and 31.06 % under visible light. The conversions of methylene blue degradation over various TiO$_2$/rGO and TiO$_2$/rGO* photocatalysts were in agreement with the results of PL and UV-Vis. Increasing the rGO content resulted in slower recombination rate of change carrier and better light absorption. Moreover, reducing the APTMS content resulted in narrower bandgap.

Field of Study:	Chemical Engineering	Student's Signature
		....
Academic Year:	2018	Advisor's Signature
		....

ACKNOWLEDGEMENTS

This thesis would be complete thanks to the following individuals.

Firstly, I would like to express my thesis advisor, Dr.Akawat Sirisuk for him encouragement, support, guidance in both thesis writing and experimentation throughout the course of this research.

Secondly, I would also very grateful to Professor Paisan Kittisuoakorn and Associate professor Kasidit Nootong of the Department of Chemical Engineering at Chulalongkorn University, and Assistant Professor Okorn Mekasuwandumrong of the Department of Chemical Engineering at Silpakorn University as my thesis committee. I am very thankful for the comments and suggestions.

Next, I would also like to thank several friends and scientists at Center of Excellence in Catalysis and Catalytic Reaction Engineering, who always giving advice, teaching the use of analytical instruments.

Finally, I most gratefully my parents for all their support and encouragement throughout the study and period of this thesis.

Sirinya Kanjanapanasont

TABLE OF CONTENTS

LIST OF TABLES

จุฬาลงกรณ์มหาวิทยาลัย

CHULALONGKORN UNIVERSITY

LIST OF FIGURES

CHAPTER 1

INTRODUCTION

Currently, water pollution is one of the major environmental problems. One of the reasons is the rapid expansion of textile and printing industries [1]. Therefore, it is necessary to treat polluted water before releasing it into the environment. But a large portion of wastewater contaminated with dyes is difficult to treat because of the complex composition and high concentration of organic substances.

In general, there are 3 methods for wastewater treatment. First, the physical treatment method separates non-soluble substances from wastewater such as filtration, screening, sedimentation, and skimming. However, these processes have high operating costs [2]. Second, the biological treatment employs microorganisms to decompose and convert organic substances matter into carbon dioxide and ammonia. Microorganisms that used to decompose organic substances such as biofilms, sludge, and granules [3] needs an optimum condition for microbial work and takes a long time to decompose. This method is not suitable for dye degradation [1, 2]. Last, the chemical treatment adds various chemicals to eliminate contaminants, but this process has many effects on the environment such as H_2O_2, chlorine, sulfate, and heavy metal [2]. However, titanium dioxide (TiO_2) photocatalysis is environmentally friendly. Therefore, this research focuses on green technology, while trying to reduce the cost of wastewater treatment. As a result, the treatment chosen by this research is photocatalytic process.

In many years, titanium dioxide is a semiconductor used in a photocatalytic process under both UV and visible irradiations. When the electron in a valence band (VB) of TiO_2 receives energy from the photon, it becomes excited from the valence band up to the conduction band (CB). Then the photogenerated electron reacts with oxygen molecule (O_2) to produce superoxide radical anions ($\cdot O_2^-$) and the product from positive hole (h^+) reaction with water molecule is hydroxyl radicals ($\cdot OH$) [4]. Both superoxide radical anions and hydroxyl radicals can promote the oxidation and dye degradation to

H_2O, CO_2, and other small molecules. The result of this reaction is that the dye in the wastewater is eliminated.

Generally, titanium dioxide (TiO_2) comprises 3 forms of polymorph in nature, namely, anatase, rutile, and brookite [5]. TiO_2 is also widely used due to its mechanical strength, long-term stability, strong oxidation ability, high activity, environmental-friendly, non-toxicity, and non-expensive [4, 6, 7]. However, TiO_2 possesses a wide bandgap [4]. Therefore, many researchers studied the improvement of TiO_2 photocatalyst for greater efficiency.

In a photocatalytic process, the photogenerated electron-hole pairs in TiO_2 semiconductor can recombine quickly [8], thereby lowering its performance. Therefore, we incorporated reduced graphene oxide (rGO) into the system by wrapping TiO_2 surface with rGO to increase its photocatalytic activity [9], improve the surface-adsorbed chemical molecules through π–π interactions [10, 11], and extend the light absorption range into visible region [12].

To synthesize TiO_2/rGO catalyst, TiO_2 surface must be modified with 3-aminopropyl-trimethoxysilane (APTMS) first. The amine group anchored on the TiO_2 surface has a positive charge and attracts rGO with a negative charge while being wrapped on the TiO_2 surface. When TiO_2 was wrapped with rGO, recombination electrons and holes become slower [9, 12].

In this research, we chose methylene blue as a model organic dye contaminant. The photocatalytic degradation of methylene blue under UV and visible irradiations in aqueous phase based on TiO_2/rGO catalyst was studied (as seen in Figure 1).
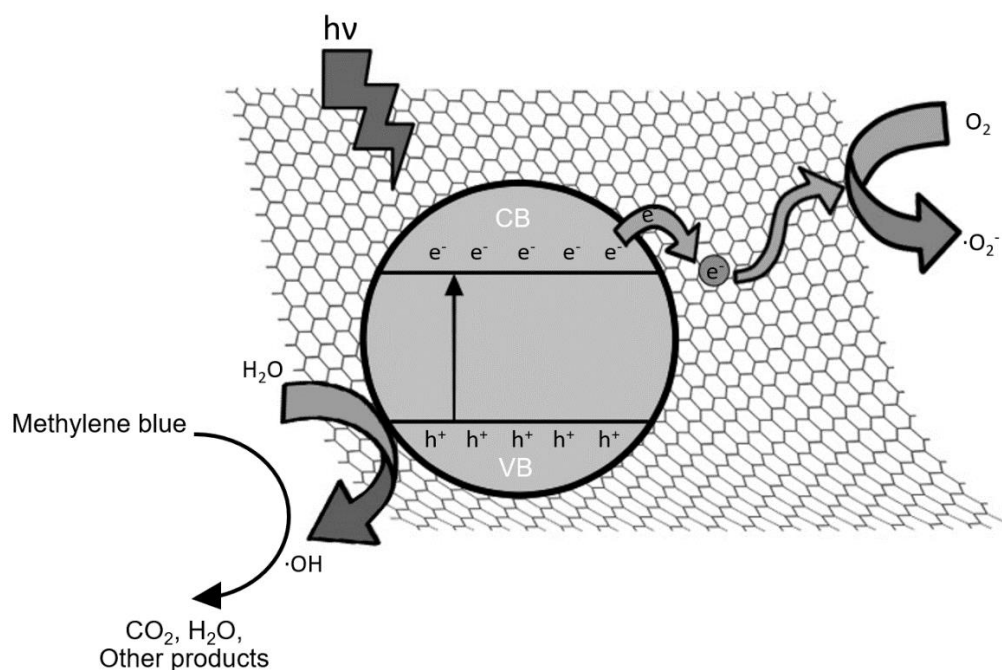
Figure 1 Schematic diagram of the proposed toward photocatalytic of methylene blue over TiO_2/rGO photocatalyst under UV or visible irradiation.

1.2 Objectives

    1. To improve photocatalytic activity of TiO_2 photocatalyst by wrapping with rGO.

    2. To investigate effects of the amount of rGO and amine group on the photocatalytic activities of the TiO_2/rGO in methylene blue degradation.

1.3 Research scopes

    1.3.1 Synthesis of titanium dioxide/reduce graphene oxide (TiO_2/rGO)

        1. TiO_2 was synthesized via a sol-gel method.

        2. GO was synthesized from graphite powder using modified Hummers method.

        3. GO was reduced to rGO with hydrazine and ammonia solution.

        4. The concentration of APTMS was varied at 2.21 and 22.1 mmol.

        5. TiO_2/rGO was prepared by heating and refluxing at 95-100°C for 24 hours.

        6. The amount of rGO was varied from 0 to 0.05 g.

1.3.2 Characterization of the TiO_2/rGO catalysts

      1. X-ray diffractometry (XRD)

      2. Nitrogen physisorption

      3. Fourier transform infrared spectroscopy (FTIR)

      4. UV-visible diffuse reflectance spectroscopy

      5. Photoluminescence spectroscopy (PL)

      6. Scanning electron microscope (SEM)

      7. Thermogravimetric analysis (TGA)

1.3.3 The photocatalytic activity testing

      1. The photocatalytic activities for methylene blue degradation in aqueous phase over TiO_2/rGO catalysts under either UV or visible irradiation were investigated.

      2. The concentration of methylene blue was measured by UV-visible spectrophotometer at the wavelength of 665 nm.

จุฬาลงกรณ์มหาวิทยาลัย

CHULALONGKORN UNIVERSITY

1.4 Research methodology

```
┌─────────────────────────────────┐     ┌─────────────────────────────────┐
│                                 │     │   Synthesis of GO by using      │
│ Synthesis of TiO₂ via a sol-gel │     │   modified Hummers method       │
│ method                          │     │                                 │
└─────────────────────────────────┘     └─────────────────────────────────┘
```

Synthesis of TiO$_2$ via a sol-gel method

Synthesis of GO by using modified Hummers method

Preparation of APTMS-TiO$_2$
(2.21:100.16 mmol)

Preparation of APTMS-TiO$_2$
(22.1:100.16 mmol)

TiO$_2$/rGO* weight ratio TiO$_2$:rGO is 1:0, 1:0.02, and 1:0.04

TiO$_2$/rGO weight ratio TiO$_2$:rGO is 1:0, 1:0.005, 1:0.01, 1:0.02, 1:0.03, 1:0.04, and 1:0.05

Characterization of the catalysts
- X-ray diffractometry (XRD)
- Nitrogen physisorption
- Fourier transform infrared spectroscopy (FTIR)
- UV-visible diffuse reflectance spectroscopy
- Photoluminescence (PL)
- Scanning electron microscope (SEM)
- Thermogravimetric analysis (TGA)

Photocatalytic degradation of methylene Blue

Discussion

Conclusion

CHAPTER 2
THEORY

2.1   Titanium dioxide

Titanium dioxide (TiO_2) or titania is commonly used in many industries including paints, cosmetics, electronics, filter coating, biomedicine, dye-sensitized solar cells and catalysts [13]. The properties of TiO_2 as seen in Table 1. In 1972, Fujishima and Honda introduced titanium dioxide as a semiconductor to photocatalytic decomposition of water splitting under UV irradiation [14].

Table 1 The chemical and physical properties of titanium dioxide (TiO_2) [13]

Molecular Formal	TiO_2
Molecular weight	79.866 g/mol
Melting point	1844 °C
Boiling point	2973 °C
Refractive index	Anatase Rutile Brookite
Appearance	White solid
Solubility	Insoluble in water
Odor	Odorless

In general, titanium dioxide has 3 crystalline phases, namely, rutile, anatase, and brookite (as seen in Table 2 and Figure 2). Rutile phase is the stable phase because anatase and brookite phases when heated can be transformed to rutile phase [6]. The stability of crystalline phases of titanium dioxide is in the order of rutile> brookite> anatase [5]. However, anatase phase of TiO_2 is more active than rutile and brookite TiO_2 phases in terms of a photocatalytic activity. Still anatase has drawback due to a larger bandgap [4].

Table 2 Types of TiO_2 polymorphs and physical properties [13].

Crystal structures	Crystal system	Density (g/cm^3)	Optical bandgap (eV)	Refractive index
Rutile	Tetragonal	4.13-4.26	3.0	2.72
Anatase	Tetragonal	3.79–3.84	3.19	2.52
Brookite	Orthorhombic	3.99-4.11	3.11	2.63

a) rutile   b) anatase   c) brookite
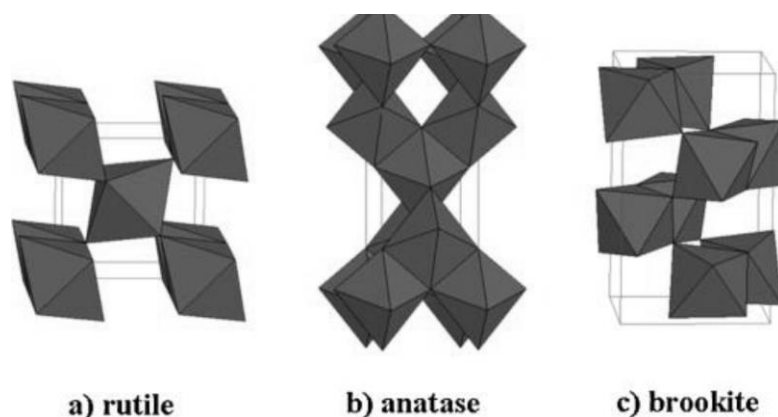
Figure 2 TiO_2 crystal structures of (a) rutile, (b) anatase, and (c) brookite [13]

In photocatalysis, when TiO_2 photocatalyst is activated by UV or visible irradiation with energy larger than bandgap energy, photogenerated electron (e^-) in the VB excited to CB and left behind a h^+ in the VB. A hole reacts with water to produce •OH, which degrades dye into CO_2, H_2O, and other products (shown in Equations (1) to (6) below) [6].

$$TiO_2 + h\mathbf{\nu} \rightarrow h^+ + e^- \tag{1}$$

$$h^+ + organic \rightarrow CO_2 \tag{2}$$

$$h^+ + H_2O \rightarrow •OH + H^+ \tag{3}$$

$$h^+ + OH^- \rightarrow •OH \tag{4}$$

$$•OH + organic \rightarrow CO_2 \tag{5}$$

$$e^- + O_2 \rightarrow •O_2^- \tag{6}$$
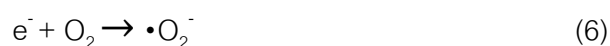
2.2 Sol-gel method

The sol-gel is a commonly method used for the synthesis of TiO_2 from precursors which solid particles (precursors) convert to colloidal solution (sol) and integrated network (gel) [15]. This method can prepare solids at low temperatures. The chemical reaction of the sol-gel method is based on hydrolysis and condensation reactions [16] as seen in Equations (7) to (9).

$$Ti(OR)_4 + 4H_2O \rightarrow 2Ti(OH)_4 + 4ROH \qquad : \text{Hydrolysis} \qquad (7)$$

$$Ti(OH)_4 + Ti(OH)_4 \rightarrow TiO_2 + 4H_2O \qquad : \text{Water condensation} \qquad (8)$$

$$Ti(OH)_4 + Ti(OR)_4 \rightarrow 2TiO_2 + 4ROH \qquad : \text{Alcohol condensation} \qquad (9)$$

Where R is alkyl group such as ethyl, i-propyl, and n-butyl

2.3 Graphene oxide

2.3.1 Structure and properties of graphene oxide

Graphene or monolayer sheet of graphite arranged in a honeycomb structure, where each carbon atom is held together by a covalent bond [17]. It is produced by the oxidation of graphite using oxidizing agent in acidic solution.

Graphene oxide (GO) has various functional groups on sheet such as hydroxyl, epoxide, and carbonyl [18]. It possesses large high surface area, attractive mechanical, electronic, thermal and optical properties.

2.3.2 Synthesis of graphene oxide

The preparation of GO from graphite as seen in Figure 3. There are 3 principal methods for synthesis of graphene oxide developed by Brodie, Staudenmeier, and Hummers, respectively.

Brodie method [19] is the first method for the synthesis of graphene oxide in 1859. Fuming nitric acid was mixed with graphite powder and potassium chlorate, an oxidizing agent, was later added. The resulting product was a mixture of graphene and graphite oxide. The elemental analysis found that the product contained 60% C, 2% H and 38% O. But this reaction is still dangerous.

Staudenmeier method [20] was improved further from Brodie's method. An acidic mixture was prepared by mixing adding sulfuric acid and potassium chlorate. Both Brodie and Staudenmaier methods have a byproduct as chloride toxic gas, which can decompose rapidly in the air, causing the explosion. But graphite is more oxidized.

For Hummers method [21], potassium permanganate and sodium nitrate are mixed with graphite in sulfuric acid. After that, hydrogen peroxide was poured into the suspension to eliminate manganese ions. In general, graphene oxide that is synthesized from this method have flakes about 1 nm and a lateral size of 1 μm.
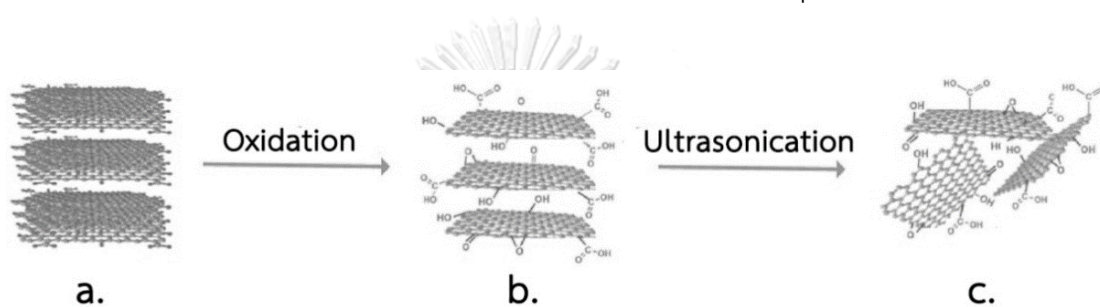
Figure 3 Schematic representation of the preparation of GO graphite, (b.) graphite oxide, and (c.) graphene oxide [9]

2.4   Reduce graphene oxide

Reduce graphene oxide (rGO) is a product of a reduction of graphene oxide by eliminating the oxygen-containing groups with the recovery of a conjugated structure by chemical reaction (see Figure 4) [12]. Several reducing agents can be used such as hydrazine [22], ammonia [23, 24], ascorbic acid [25], and sodium borohydride [26]. The rGO can be applied in battery [27], dye-sensitized solar cell [28], biosensor [29], and catalyst [9, 30-33].
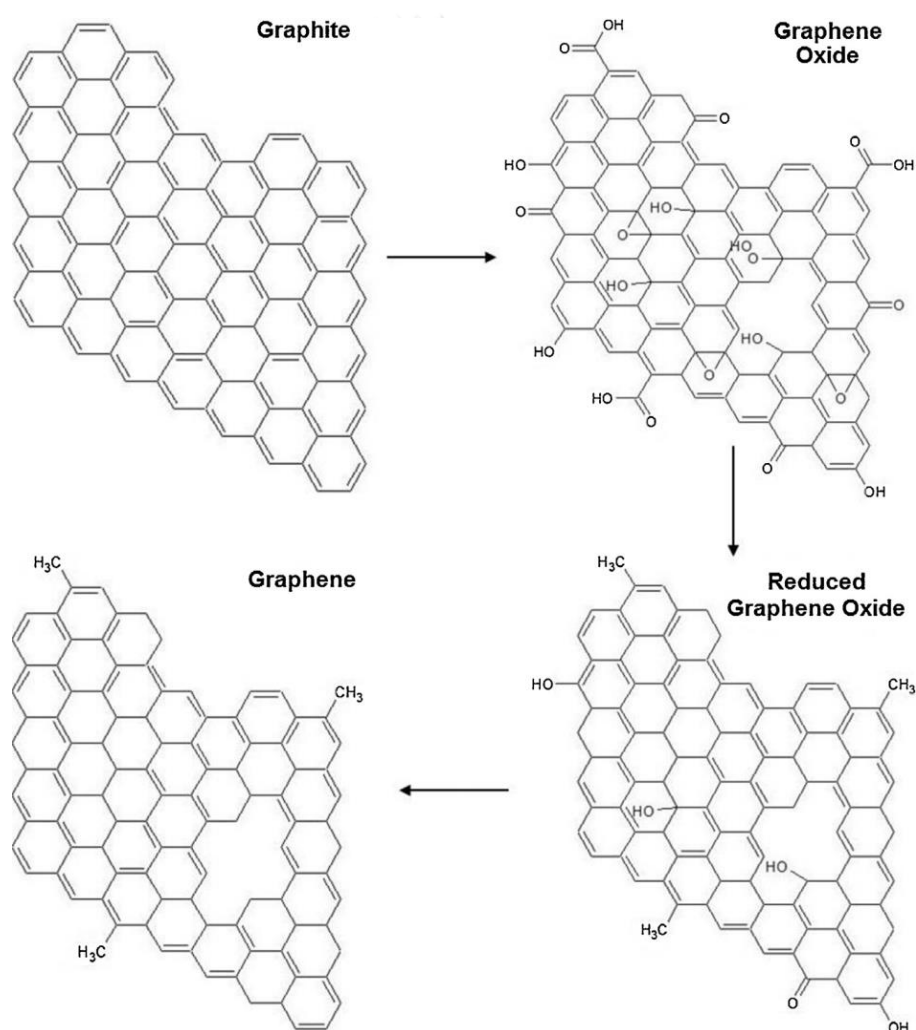
Figure 4 Chemical structures of graphite, graphene oxide and reduced graphene oxide and graphene [34].

2.5   3-Aminopropyl-trimethoxysilane

The compounds, 3 - aminopropyl-trimethoxysilane (APTMS) has a molecular weight of 179.29 g/ mol (see Figure 5). In general, APTMS is often used to modify the surface of the catalyst to enhance its performance, such as TiO_2 [10, 35], Fe_3O_4 [36], ZnO [37], and MCM-41 [38].
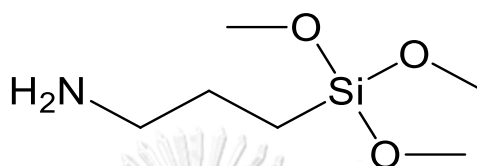
Figure 5 Structure of 3-aminopropyl-trimethoxysilane

2.6   Methylene blue

2.6.1   Structure and properties of methylene blue

Methylene blue is a dye commonly used in the textile industry, which is classified as a heterocyclic aromatic compound with chemical name 3,7-bisdi-methylamino phenazathionium chloride trihydrate ($C_{16}H_{18}ClN_3S \cdot 3H_2O$) (see Figure 6) [39]. It has a dark blue-green color. Sometimes called this type of dye is cationic thiazine dye. It is widely used in a number of areas such as medicine, biology, and chemical indicator. In human, methylene blue is toxic if received in large quantities and the body will be affected such as increased heart rate, vomiting, chest pain, shock, and bluish discoloration of skin [40].
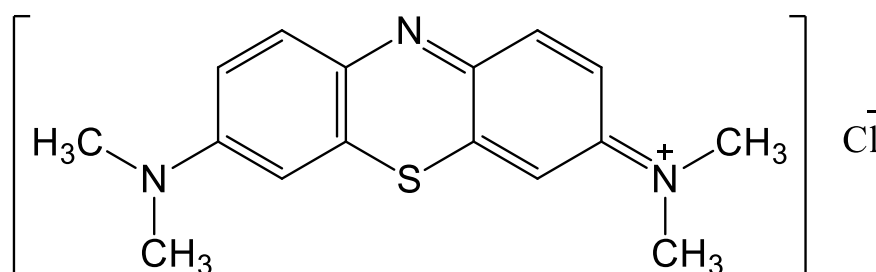
Figure 6 Structure of methylene blue

2.7 Photocatalytic degradation pathway of methylene blue

The pathway for the photocatalytic degradation of methylene blue dyes by TiO_2 is shown in Figure 7. The decomposition products are detected by GC/MS and LC/MS [41].
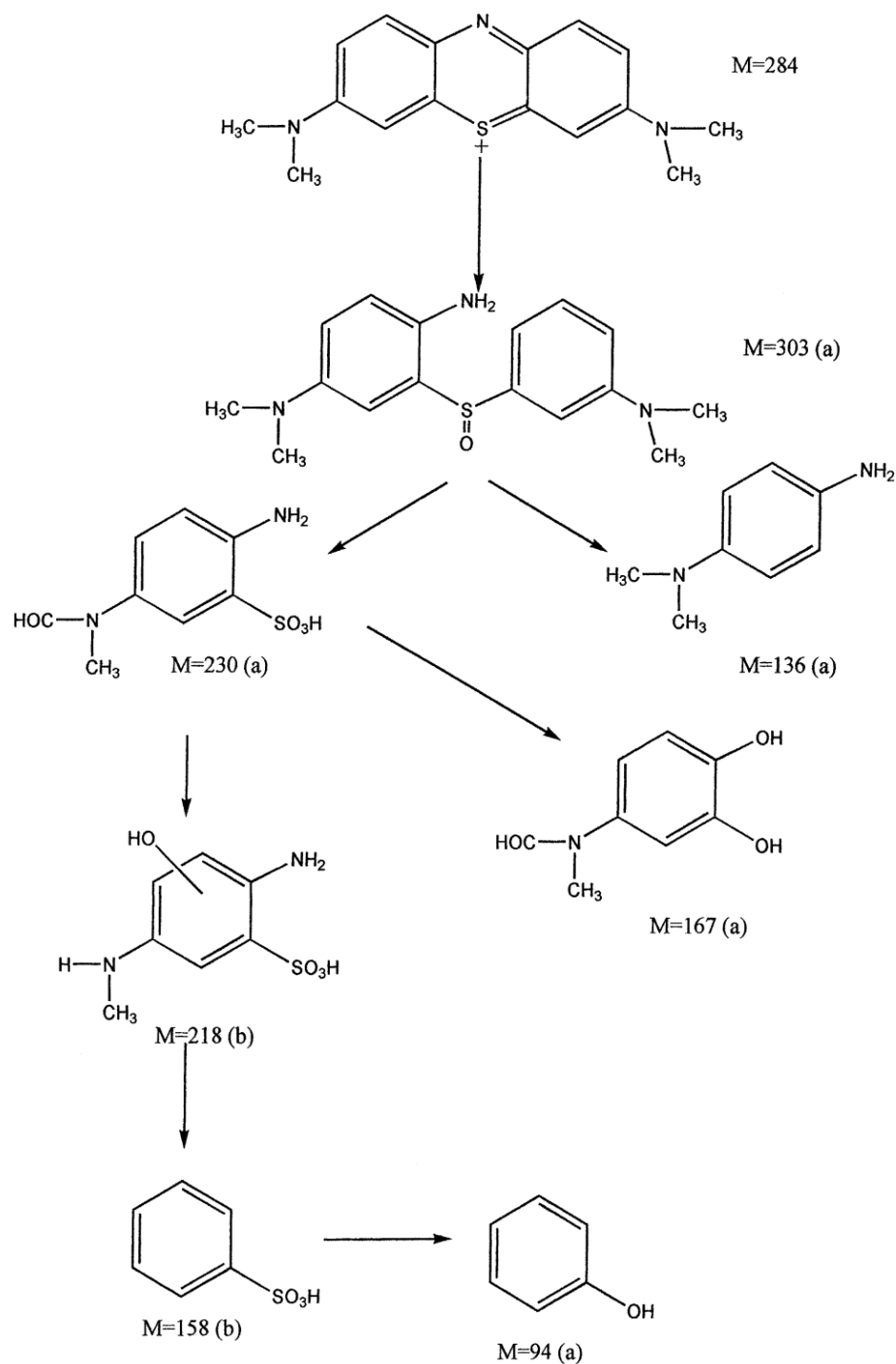
(a) detected by GC/MS (extraction of ions)
(b) detected by LC / MS

Figure 7 Photocatalytic degradation pathway of methylene blue [6]

CHAPTER 3
LITERATURE REVIEWS

3.1   Effects of amine group added to titanium dioxide on properties

Klaysri et al. [35] studied the effect of 3-aminopropyltriethoxysilane (APTES) used to modified the surface of TiO_2 on conversions of methylene blue decolorization under visible irradiation. The APTES-TiO_2 catalysts investigated contained APTES at 0.1, 1.0, and 10 mM. The 0.1 mM APTES-TiO_2 exhibited the highest conversion because the monolayer of aminosilane coverage on TiO_2 surface narrowed the bandgap, resulting in a decrease in rate of electron-hole recombination.

Iijima et al. [42] studied the effect of ratio of mixed silane alkoxides on reactivity with TiO_2 nanoparticle surface and stability in organic solvents. Hydrophilic TiO_2 nanoparticles were synthesized using a mixture of decyltrimethoxysilane/3-aminopropyltrimethoxysilane (DTMS/APTMS) and phenyltrimethoxysilane/3-aminopropyltrimethoxysilane (PTMS/APTMS) by varying the amount of DTMS, APTMS, and PTMS. As a result, during the modification process, the pH value increased when APTMS was added to TiO_2 nanoparticle suspension. Highly hydrophobic silane ratio of TiO_2 can re-dispersible into low-polar solvents such as hexane, toluene, and THF. By the addition of hydrophilic silanes to TiO_2 surface, hydrophilic TiO_2 nanoparticles were dispersible in highly polar solvents such as NMP, DMAc, and DMSO.

Fadillah et al. [43] investigated the effect of surface modification TiO_2 nanorods with APTMS. This research successfully grafted amine group onto TiO_2 surface by Ti-O-Si chemical bonds. The N3 complex-APTMS enhanced the visible light absorption of TiO_2. TiO_2, TiO_2-APTMS 5%, TiO_2-APTMS 10%, and TiO_2-APTMS 15% were studied and the best result was obtained from 10 % (v/v) APTMS in terms of efficiency of dye-sensitized solar cell.

Kominami et al. [44] modified the surface of TiO_2 with APTMS for nitrogen oxides (NO_x) removal. As a result, modification with APTMS inhibited TiO_2 crystal growth and transformation of anatase to rutile TiO_2 during the calcination process, resulting in improved thermal stability of the support. The V_2O_5/TiO_2 catalyst had a strong interaction between the protonated amino group in the modified TiO_2. The V_2O_5/TiO_2 catalyst, of which the surface was modified with APTMS had a large surface area and higher activity than the V_2O_5/TiO_2 prepared from an unmodified catalyst (as seen in Figure 8).
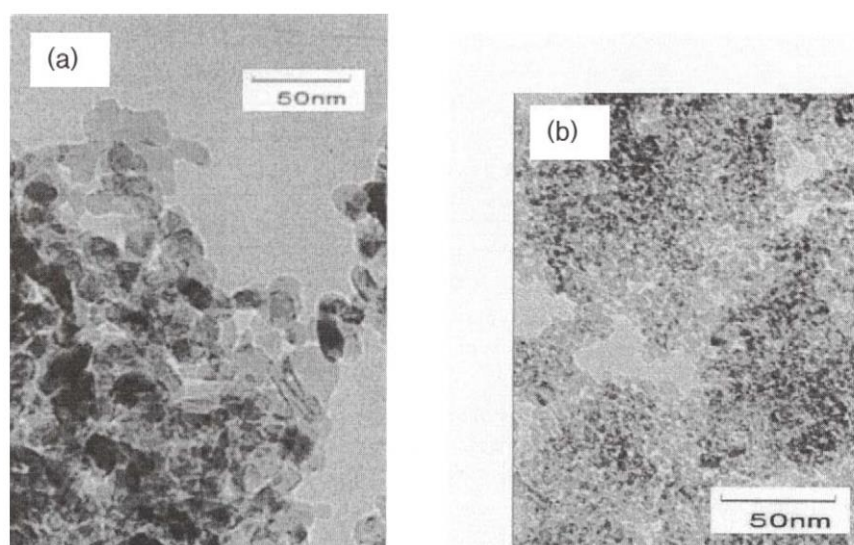
Figure 8 TEM photographs of samples after calcination of (a) unmodified TiO_2,
(b) APTMS-TiO_2 at 550 °C [44]

Zhao et al. [45] investigated the effect of surface modification with 3-aminopropyltrimethoxysilane (APTMS) and 3-isocyanatopropyltrimethoxysilane (IPTMS) on surface properties of TiO_2 nanoparticles. As the ratio of organosilane was increased from 0 %wt to 200 %wt, the rate constant for APTMS-TiO_2 photocatalytic activity was slightly lower. On the other hand, the rate constant for IPTMS-TiO_2 quickly dropped because IPTMS is more effective in grafting than APTMS.

Pasqui et al. [46] studied the preparation of self-cleaning textile fabrics by TiO_2 nanoparticles grafted polyester fibers. In sample preparation, TIO_2 surface was modified first with the APTMS so that the Si-O-Ti bond has interacted with polyester fibers.

Therefore, APTMS-TiO_2 was grafted with polyester fibers. From the results, the sample was effective in removing methylene blue stains well within 3 hours under UV irradiation.

3.2   Effects of GO and rGO in a photocatalytic process

Sun et al. [47] studied of the application of rGO in various G/TiO_2, G/ZnO and G/Ta_2O_5 composite photocatalyst and investigated the photocatalytic activities of the composites for the photodegradation of methylene blue under UV–vis and visible light. For the results of the degradation of methylene blue in visible light, graphene enhanced the activity in the visible region in G/TiO_2 catalyst greater than other composites. For the degradation of methylene blue under UV-vis light with TiO_2 and $G-TiO_2$ catalysts decomposed 100% of methylene blue after 110 minutes. The ZnO and G/ZnO catalysts degraded methylene blue 100% under UV-vis light after 30 and 60 minutes respectively, which were more efficient than TiO_2 and G/TiO_2 catalysts. On the other hand, they had low efficiencies under visible light. Next, the Ta_2O_5 and G/Ta_2O_5 catalysts degraded 50.2 and 72.1% of methylene blue after 120 minutes under UV–vis light but the $G-Ta_2O_5$ catalyst was not very active in degrading methylene blue under visible light because it has a wide bandgap of 3.67 eV (as seen in Figure 9).
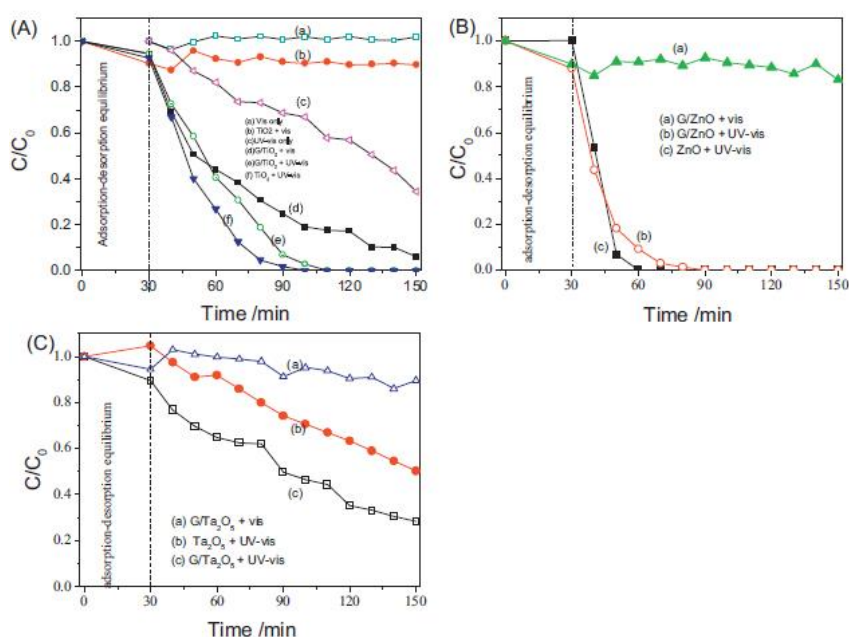
Figure 9 Photocatalytic oxidation of methylene blue at various conditions.

(A) TiO_2 and G/TiO_2, (B) ZnO and G/ZnO, and (C) Ta_2O_5 and G/Ta_2O_5 [47]

Ni et al. [10] studied the effect of rGO wrapping on the surface of highly-reactive anatase by modifying the surface of TiO_2 via a hydrothermal method. The structure of rGO wrapped TiO_2 is called a core-shell structure. This structure lessened the bandgap more than the rGO-supported TiO_2. The performance was investigated by photodegradation of methylene blue under UV and visible irradiation.

Zou et al. [48] studied the effects of congo red degradation by CdS-rGO nanocomposites under simulated sunlight irradiation. The photocatalytic activity and stability of CdS-rGO nanocomposites was improved, compared with CdS nanoparticles and CdS/GO mixture because rGO sheets enhanced light conversion efficiency, decrease the recombination of electron-hole pairs, and promote the charge separation.

Amaranatha et al. [49] studied the enhanced photocatalytic activity of ZnS-Ag_2S wrapped with rGO in degrading rhodamine B solution under simulated sunlight irradiation. The ZnS-Ag_2S-rGO nanocomposite was synthesized by hydrothermal method without any surfactant. The photocatalytic ability of ZnS -Ag_2S-rGO nanocomposite was the highest among ZnS, ZnS-rGO, Ag_2S, Ag_2S-rGO, and ZnS-Ag_2S. As a result, rGO sheet which has good conductivity, facilitated the charge transfer between ZnS to Ag_2S, thereby increasing the photocatalytic ability of ZnS-Ag_2S-rGO nanocomposite.

Li et al. [30] investigated the effect of gold and various amounts of rGO added to TiO_2 catalyst. TiO_2, Au/TiO_2, and $TiO_2/Au@rGO$ hybrids were synthesized and used the decomposition of methyl orange under UV and simulated solar light. GO was reduced to rGO via hydrazine and ammonia. The $TiO_2/Au@rGO$ hybrids promoted multi-channel electron transfer paths, resulting in the best performance compared to TiO_2 and Au/TiO_2. And the amount of rGO added in the range of 0.25-0.75 %w/w provides the highest efficiency. On the other hand, an increase in rGO, decreased the degradation of methyl orange because the excessive rGO was obscuring the light.

CHAPTER 4
EXPERIMENTAL

This chapter describes the detail of chemicals and methods used in catalytic preparations, photocatalytic test, and characterization of catalyst.

4.1   Materials and chemicals

Table 3 List of chemicals in this research

Chemicals	Formula	Brand
Graphite	C	Fluka
Sodium nitrate	$NaNO_3$	Fluka
Sulfuric acid	H_2SO_4	Merck
Potassium permanganate	$KMnO_4$	Suksapanpanit
Hydrogen peroxide	H_2O_2	Aldrich
Hydrochloric acid	HCl	Qrec
Ethanol	CH_3CH_2OH	Merck
Methanol	CH_3OH	RCI Labscan
Titanium(IV)isoproproxide	$TiOCH(CH_3)_{24}$	Aldrich
Nitric acid	HNO_3	RCI Labscan
(3-Aminopropyl)trimethoxysilane	$H_2N(CH_2)_3Si(OCH_3)_3$	Aldrich
Hydrazine solution	N_2H_4	Aldrich
Ammonia solution	NH_3	Qrec
Toluene	$C_6H_5CH_3$	Merck
Diethyl ether	$(C_2H_5)_2O$	Merck
Methylene blue	$C_{16}H_{18}N_3ClS \cdot 2H_2O$	UNILAB

4.2   Preparation of TiO$_2$/rGO catalyst

4.2.1   Synthesis of GO

GO was synthesized using a modified Hummers method. In a typical synthesis procedure, 50 mL of concentrated sulfuric acid was cooled to 4 °C in an ice bath. Then

2.0 g of graphite powder and 1.0 g of NaNO$_3$ were added to the concentrated H$_2$SO$_4$. Next, KMnO$_4$ was put gradually into a mixture while being stirred for 2 hours. Then the mixture was stirred continuously at room temperature for 30 minutes. After that, 100 mL of deionized (DI) water was poured carefully into a mixture. The mixture was slowly heated to 90 °C under constant stirring for 3 hours. Later, 50 mL of 5% H$_2$O$_2$ solution was added to eliminate residual MnO$_4^-$ and the mixture was stirred for 1 hour. Finally, GO aqueous suspension was centrifuged, washed by 5% HCl, DI water and ethanol several times until the pH of rinse water became neutral. The product was dried at 60 °C in oven overnight.

4.2.2 Synthesis of TiO$_2$ nanoparticles [50]

The first step in the synthesis of TiO$_2$ via a sol-gel method was pouring the 1000 mL of DI water into the flask. After that, 83.33 mL of titanium(IV)isoproproxide was added to the solution. Then 7.25 mL of 65% HNO$_3$ was added and the mixture became milky suspension. The suspension was stirred continuously for 3 days until the mixture became clear. Next, the sol was dialyzed inside cellulose membranes with a molecular weight cutoff of 3500 in DI water until the pH value reached 3.8. Finally, the sol was dried, crushed, and calcined at 400 °C for 2 hours with a heating rate 10 °C /minutes.

4.2.3 Surface modification of TiO$_2$ with APTMS [44]

In this process, 8.0 g of TiO$_2$ was dispersed in 80 mL of anhydrous toluene with the assistance from ultrasonication for 30 minutes. The concentrations of APTMS, we were investigated in were 2.21 and 22.1 mmol. The reaction mixtures were then refluxed at 110 °C and stirred for 8 hours. After that, the mixtures were centrifuged and washed with toluene, diethylether, and methanol to remove other residual chemicals. Ultimately, modified particles were dried in oven at 60 °C in oven overnight. The products were represented as APTMS-TiO$_2$ (2.21 mmol) and APTMS-TiO$_2$ (22.1 mmol), respectively.

4.2.4   Fabrication of TiO_2/rGO catalyst

In the synthesis of TiO_2/rGO catalysts. The surface of TiO_2 was wrapped with rGO according to the following steps. Initially, different amount of GO (0, 0.005, 0.01, 0.02, 0.03, 0.04 and 0.05 g) was dispersed into 500 mL of deionized water under sonication for 30 minutes. This process dispersed the layers of graphite oxide to produce graphene oxide sheets [51]. After that, 1.0 g of APTMS-TiO_2 (22.1 mmol) powder was dispersed in GO suspension and kept sonicated for 30 minutes. In the reduction process of GO to rGO, 35% hydrazine in water solution and 28% ammonia in water solution were added in GO suspension using the volumetric ratio of hydrazine:ammonia of 0.5:3.5 [24, 52]. After heating and refluxing at 95-100 °C for 24 hours, the mixture was separated by centrifugation and was washed with DI water and absolute alcohol several times, and finally dried at 60 °C for 24 hours. The final products were referred to as TiO_2/rGO (1:0), TiO_2/rGO (1:0.005), TiO_2/rGO (1:0.01), TiO_2/rGO (1:0.02), TiO_2/rGO (1:0.03), TiO_2/rGO (1:0.04), and TiO_2/rGO (1:0.05). The synthesis of TiO_2/rGO* catalysts with APTMS-TiO_2(2.21 mmol) followed a similar procedure but the amounts of rGO were varied from 0, 2, and 4 g and were referred to as TiO_2/rGO (1:0)*, TiO_2/rGO (1:0.02)* and TiO_2/rGO (1:0.04)*, respectively.

4.3   Photocatalytic experiments

The photocatalytic activity of the TiO_2/rGO catalyst was investigated by measuring the conversion of methylene blue for the photodegradation under UV and visible light irradiations at room temperature. First, 400 mL of methylene blue (10 mg/L) solution was charged in the double jacketed glass reactor. Then 0.4 g of catalyst was dispersed by stirring continuously. The system was kept in the dark for 1 **hour** to establish the adsorption-desorption equilibrium of methylene blue. Afterward, the suspension was irradiated by either UV irradiation using 75W UV-C lamp or visible light irradiation using 18W TL-D standard colors lamp (as seen in Figure 10). During the reaction, 5 mL of methylene blue solution was collected every 15 minutes for 3 **hours**. The concentration of methylene blue was measured using a UV-Vis spectrophotometer with a maximum

absorption wavelength of 665 nm. The percentage of degradation was calculated with the following equation given below:

$$\%\text{Degradation} = \frac{C_0 - C_t}{C_0} \times 100 \tag{7}$$

Where C_0 is the initial concentration of methylene blue and C_t is the concentration of methylene blue after treatment with TiO_2/rGO photocatalyst.
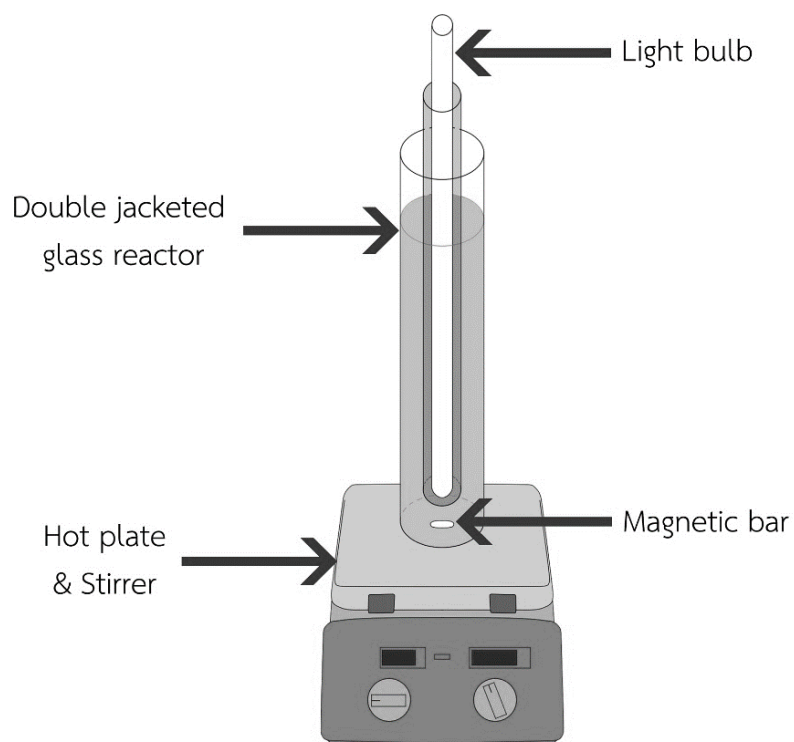
Figure 10 Photocatalysis reaction experimental setup

4.4   Catalyst characterization

4.4.1   X-ray diffractometry (XRD)

The X-ray diffraction (XRD) patterns were obtained using an X-ray diffractometer (Bruker D8 Advance) with a CuKα irradiation source and at the angle range between $20°$ to $80°$ with a scan speed of 0.5 sec/step and a receiving slit with 0.6 mm width.

The crystallite size was calculated using the Scherrer equation [53] given below:

$$D = \frac{k\lambda}{\beta \cos\theta} \qquad (10)$$

Where D is the size of the particle, λ is the X-ray wavelength (For CuK$_\alpha$ radiation using 1.54439 Å), β is the pure diffraction broadening, and θ is the diffraction angle of the peak, and k is the crystallite shape factor.

4.4.2   Nitrogen physisorption

The surface area and pore volume of catalysts were measured in a Micromeritics ASAP 2020 instrument. This analysis using 30% nitrogen gas in helium gas as a carrier gas and used liquid nitrogen in adsorption process. Generally, 0.05 g of the catalyst was placed inside the glass cell. Before analyzing, all samples were heated at 110 °C for 24 hours.

4.4.3   Fourier transform infrared spectroscopy (FTIR)

The FTIR spectroscopy, which is a technique used to identify functional groups of catalysts, were obtained under an ATR mode in the wavelength 4000-400 cm^{-1} region. The FTIR spectra of catalysts were obtained using a Thermo Scientific Nicolet 6700 FT-IR spectrometer.

4.4.4   UV-visible spectroscopy

The UV-visible spectroscopy measures the intensity of light absorbed after it passes through sample in the wavelength range from 200-800 nm. This technique measured the concentration of methylene blue. The concentration of methylene blue collected after the photocatalytic reaction at different time periods were measured by Perkin Elmer Lambda 650 spectrophotometer at the wavelength of 665 nm.

The UV-vis spectrum was also used to calculate the band gaps of semiconductor material (see Appendix D).

4.4.5   Photoluminescence spectroscopy (PL)

Photoluminescence spectroscopy investigated the charge separation of photogenerated electron and hole as well as charge-carrier lifetimes of semiconductors. The sample was excited using a Xenon lamp with an excitation wavelength of 325 nm at room temperature by Horiba Fluoromax-4P spectrofluorometer.

4.4.6   Scanning electron microscope (SEM)

SEM was used to study the morphology of the materials using JEOL model JSM-5800LV. Before analysis, the sample was heated at 110 °C overnight. After that, SEM samples were loaded on carbon tape and coated by platinum.

4.4.7   Thermogravimetric analysis (TGA)

TGA is a technique used to determine the thermal stability of materials. The sample was analyzed by a TA Instrument SDT-Q600 DSC-TGA in an air atmosphere. The temperature of the analysis was run from 30-1000 °C.

CHAPTER 5.1

RESULTS AND DISCUSSION OF SYNTHESIS

OF GRAPHENE OXIDE AND REDUCED GRAPHENE OXIDE

The results and discussion in chapter 5.1 are classified into two major parts. In the first part, several characterization techniques for the GO and rGO including TGA, UV-vis, FTIR, and SEM-EDX are described. The second part describes the adsorption of methylene blue on rGO in the dark. The decrease in concentration of methylene was detected by UV-Vis spectrophotometer.

5.1.1 Characterization of the graphene

5.1.1.1 TGA analysis

TGA analysis detected the weight loss of the GO and rGO. The sample was heated under air atmosphere. The weight loss was observed around 100 °C which was attributed to evaporation of adsorbed water. A significant weight loss occurred at 200 °C from decomposition of oxygen-containing functional group of GO. A severe weight loss of rGO in a temperature range of 500-600 °C was a result of the destruction of carbon skeleton (carbonyl and double bond) in graphene [54]. Based on the result, rGO exhibited higher thermal stability than GO because rGO contained fewer oxygen-containing functional groups than GO did.
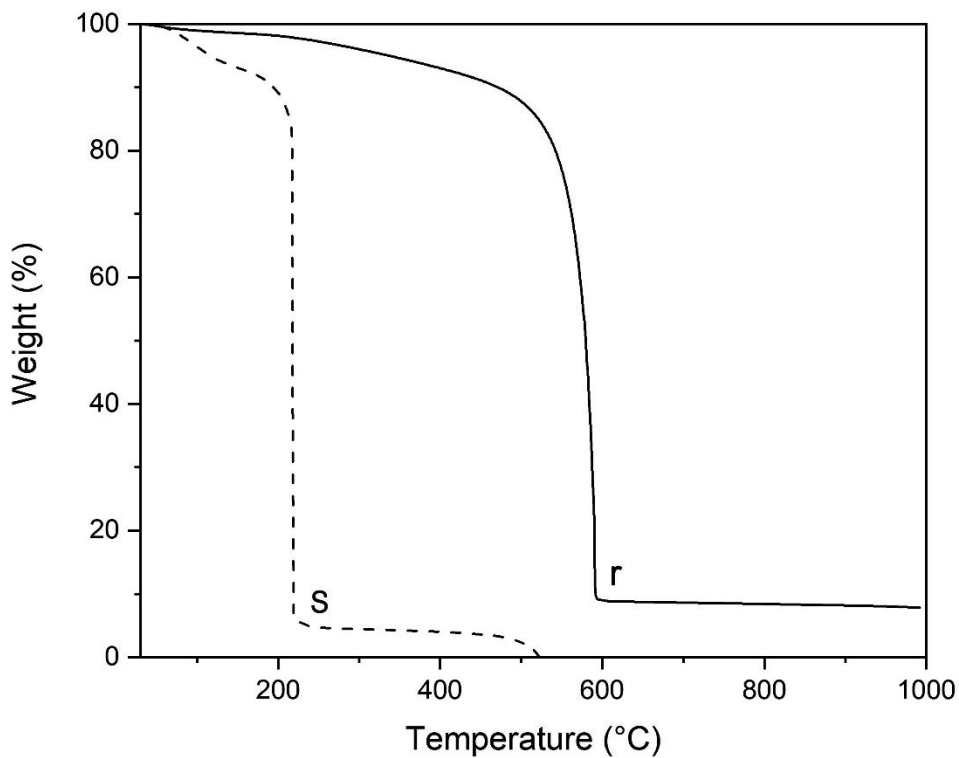
Figure 11 TGA of (s) GO and (r) rGO

5.1.1.2 Light absorption properties

To compare the light absorption performance of GO and rGO, the samples were exposed to light in the wavelength range of 200–800 nm (see Figure 12). Because the structure of GO had aromatic C=C bonds and C bonds that reacted with oxygen groups, the absorbance of GO was lower [55]. When GO reduced to rGO, there was a decrease in the amount of oxygen group in the structure. The rGO absorption value became greater. Therefore, rGO was more suitable than GO to be incorporated into the photocatalyst.
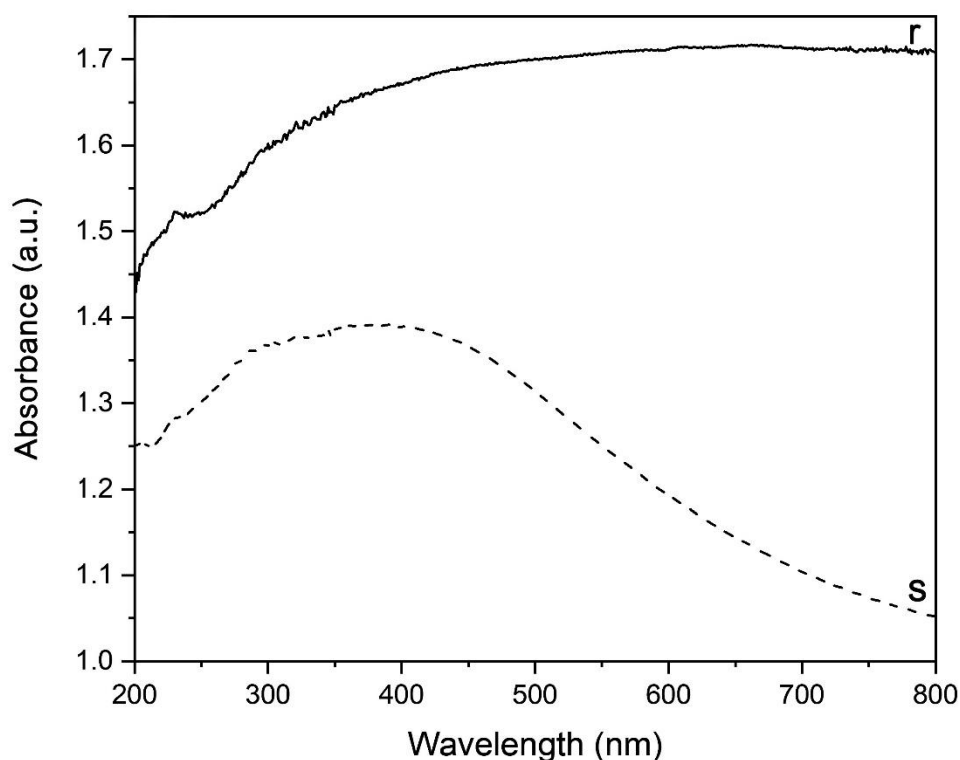
Figure 12 UV-vis spectra of (s) GO and (r) rGO

5.1.1.3 FTIR analysis

The FTIR spectra identified the functional groups in GO and rGO as seen in Figure 13. In the synthesis of GO from graphite by modified Hummer's method, In Figure 13(s) a broad brand was observed at 3234.1 cm^{-1}, which corresponded to OH stretching vibration [56]. The peak at 1717.1 cm^{-1} was assigned to the stretching vibration of C=O group [57]. The band observed at 1371.6 cm^{-1} and 1061.2 cm^{-1} corresponded to C-OH and C-O respectively ［58］. In addition, the strong peak at the 1623.1 cm^{-1} corresponded to C=C stretch [59]. After GO reduction to rGO, the peak of oxygen-containing groups (O-H, C=O, and C=O) were weakened or disappeared, which suggested that oxygenic groups were eliminated (as seen in Figure 13(r)) [60].
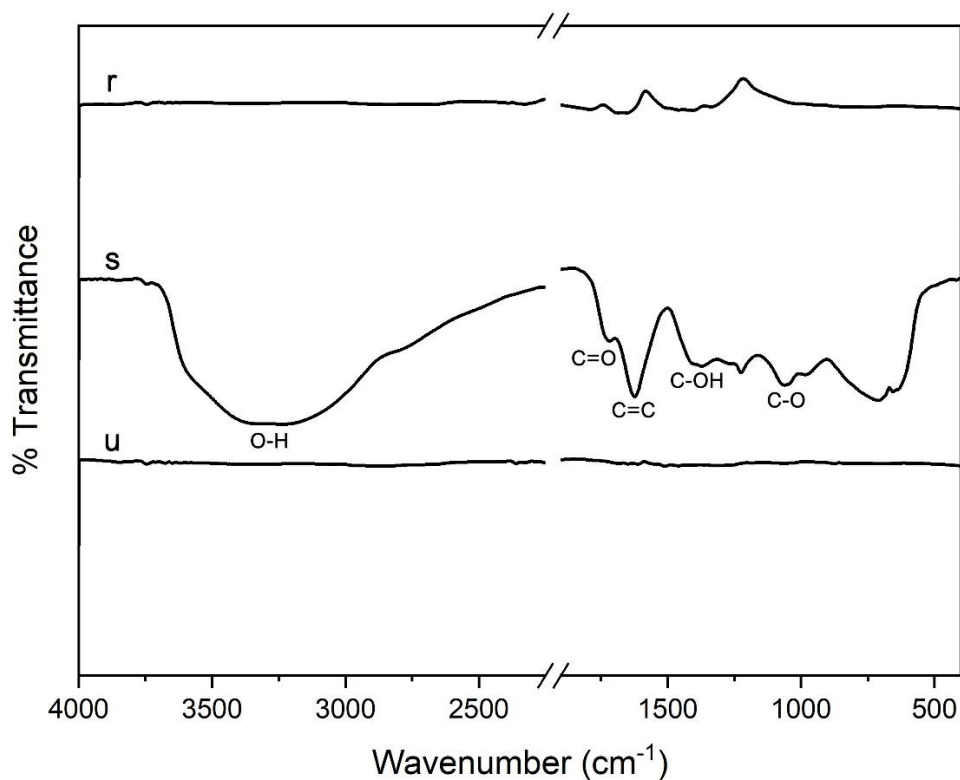
Figure 13 FTIR spectra of (u) graphite, (s) GO, and (r) rGO

5.1.1.4 Morphological features

The SEM image shows the morphology of graphite, GO, and rGO as seen in Figure 14. Figure 14(a) shows the layers of graphite that were stacked. As shown in Figure 14(b)-(c), GO and rGO possessed rough and flaky texture and each sheet was separated from one another. As GO and rGO appeared similar in morphology, energy dispersive X-ray spectroscopy (EDX) was used to study different elements on the surface. The atomic composition from SEM-EDX analysis of graphite, GO and rGO was listed in Table 4, The GO contained more oxygen atoms compared to graphite. The rGO contained fewer oxygen atoms compared to GO because oxygen-containing functional groups were removed from the structure during the reduction of GO to rGO. The SEM-EDX results suggested a successful rGO synthesis.
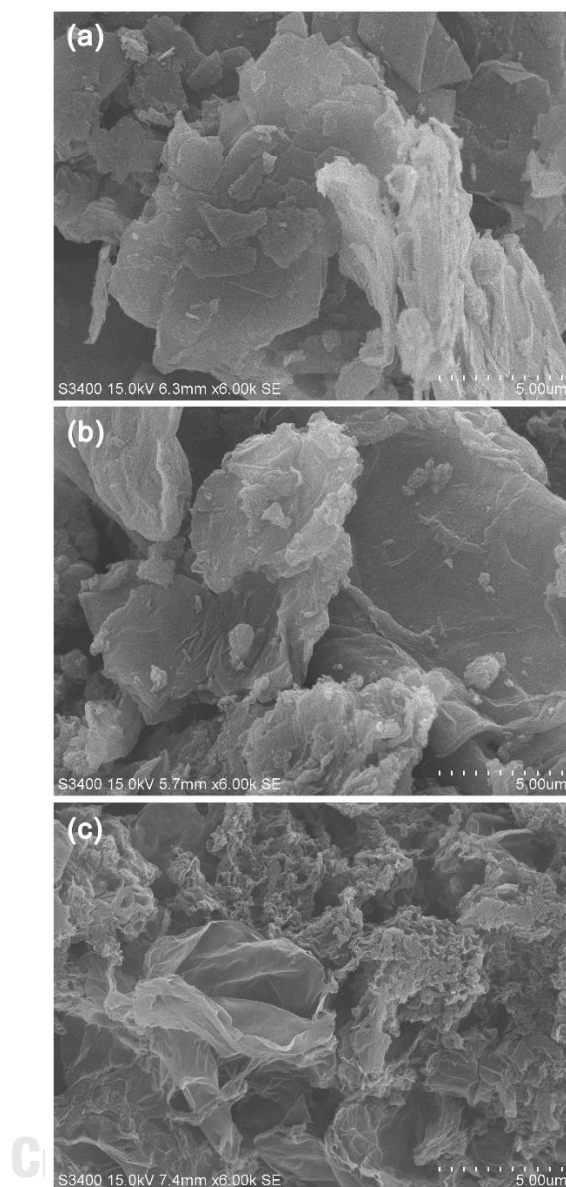
Figure 14 SEM images (magnification: 6k) of (a) graphite, (b) GO, and (c) rGO

Table 4 Summarization of each atomic surface from SEM-EDX analysis of graphite, GO, and rGO

Sample	%C	%O
graphite	99.12	0.88
GO	67.22	32.78
rGO	89.94	10.14

5.1.2 Adsorption of methylene blue on rGO

    5.1.2.1 The adsorption of methylene blue in the dark

Figure 15 shows the adsorption of methylene blue in the dark. The solution was stirred continuously for 4 hours to determine the time required for adsorption equilibrium. The result indicated that after 1 hour, the adsorption of methylene blue reached a steady level. Therefore, the period of adsorption equilibrium in this experiment was chosen as 1 hour.
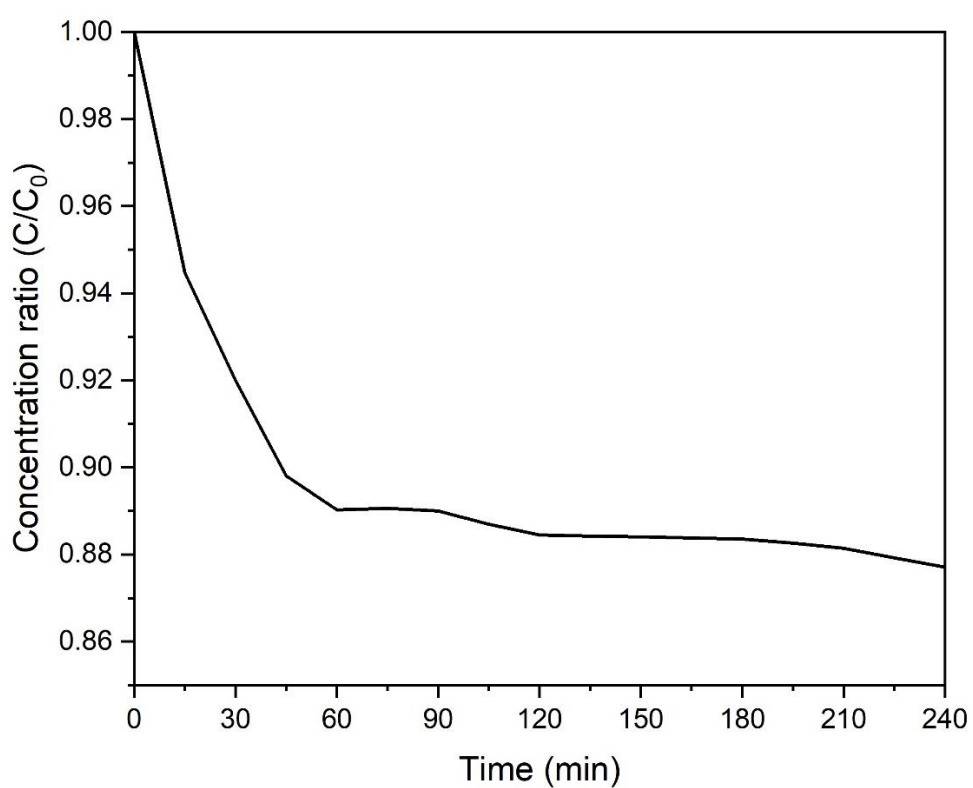
Figure 15 Adsorption of methylene blue in the absence of light using rGO

CHAPTER 5.2

RESULTS AND DISCUSSION

OF VARYING THE AMOUNT OF RGO IN THE CATALYSTS

The results and discussion in chapter 5.2 investigated the effects of different amount of rGO in TiO_2/rGO catalysts. In the synthesis of TiO_2/rGO catalysts, APTMS-TiO_2 (22.1 mmol) was synthesized with the same amount as the research relevant [44]. This chapter are divided into two major parts. In the first part, several characterization techniques for the TiO_2 and TiO_2/rGO catalysts including UV-vis, PL, FTIR, XRD, N_2 physisorption and SEM are described. And in the second part, the photocatalytic performance degradation of methylene blue under UV and visible irradiation are discussed.

5.2.1 Characterization of the TiO_2 and TiO_2/rGO catalysts

5.2.1.1 Optical absorption properties

To compare the optical absorption properties of TiO_2 and TiO_2/rGO catalysts that contained different amounts of rGO, the samples were analyzed by UV-visible spectroscopy in the wavelength range of 200-800 nm. As shown in Figure 16(p), TiO_2 exhibited strong absorption in the UV region (200-400 nm), but very weak absorption in the visible region (400-700 nm). Figure 16(a)-(g) shows that when APTMS-TiO_2 (22.1mmol) was wrapped with rGO, the light absorption in the visible region was enhanced. TiO_2/rGO catalysts exhibited better absorption properties in the visible region than TiO_2 and APTMS-TiO_2 did because rGO contained -C=C- bonds, a chromophore, that showed good absorption in the UV and visible regions. Therefore, an increase in rGO in the catalyst brought about greater absorption than APTMS-TiO_2 (22.1 mmol) and TiO_2.
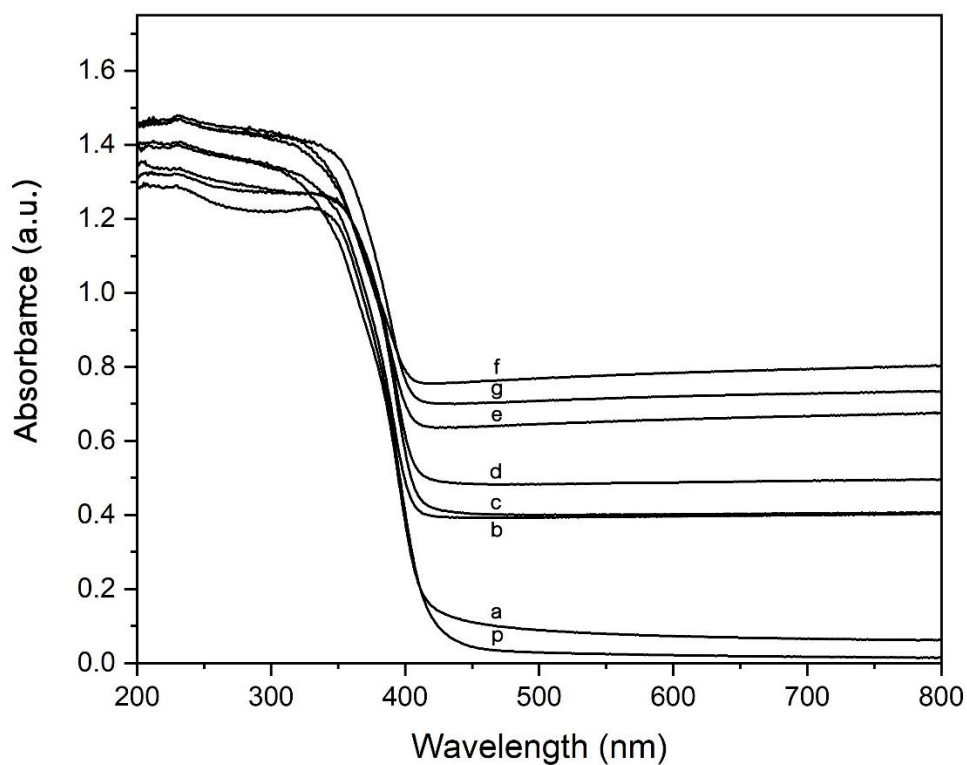
Figure 16 UV–Vis spectra of (p) TiO_2, (a) TiO_2/rGO (1:0), (b) TiO_2/rGO (1:0.005),
(c) TiO_2/rGO (1:0.01), (d) TiO_2/rGO (1:0.02), (e) TiO_2/rGO (1:0.03), (f) TiO_2/rGO (1:0.04),
and (g) TIO_2/rGO (1:0.05)

Moreover, the bandgap of TiO_2 and TiO_2/rGO catalysts could be calculated from UV-vis spectra (as seen in Appendix F). The bandgap of the TiO_2 and TiO_2/rGO catalysts were estimated from Figure 17 and was listed in Table5. The bandgap of TiO_2 is 3.06 eV, similar to the bandgap of TiO_2/rGO (1:0). When rGO was added to APTMS-TiO_2, the bandgap became slightly narrower because rGO had π-conjugated structure leading to good light absorption. The narrower bandgap resulted in the catalyst that absorbed more light in the visible region and exhibited good photocatalytic activity.
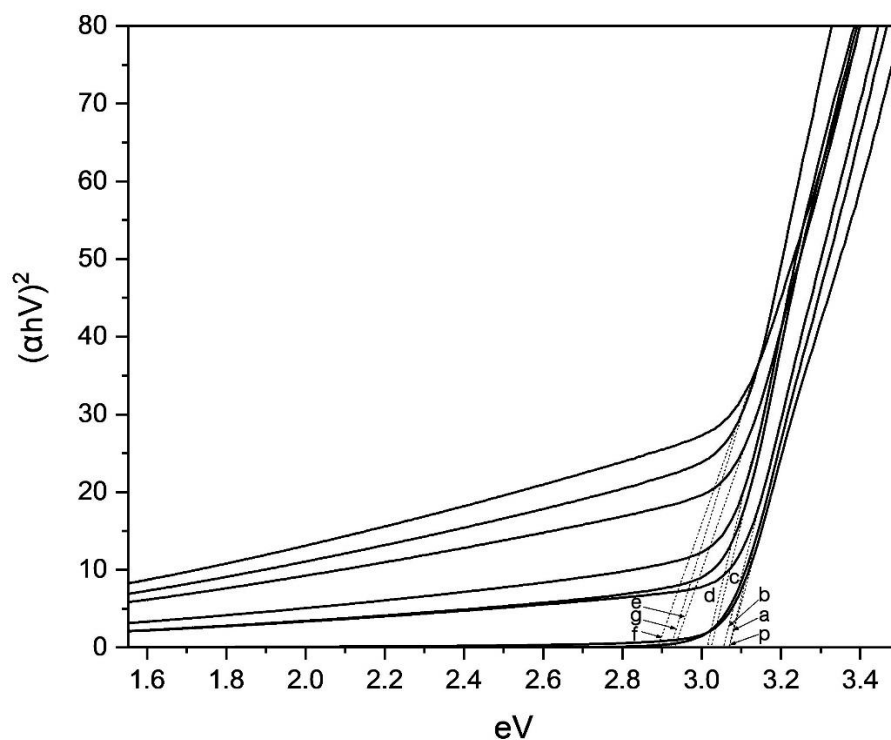
Figure 17 Plot of the bandgap, as derived from the diffuse reflectance UV–Vis spectra
of (p) TiO_2, (a) TiO_2/rGO (1:0), (b) TiO_2/rGO (1:0.005), (c) TiO_2/rGO (1:0.01),
(d) TiO_2/rGO (1:0.02), (e) TiO_2/rGO (1:0.03), (f) TiO_2/rGO (1:0.04),
and (g) TIO_2/rGO (1:0.05)

Table 5 The comparison bandgap from UV-vis spectra of TiO_2 and TiO_2/rGO catalysts

Sample	Bandgap (eV)
TiO_2	3.06
TiO_2/rGO (1:0)	3.06
TiO_2/rGO (1:0.005)	3.05
TiO_2/rGO (1:0.01)	3.02
TiO_2/rGO (1:0.02)	2.99
TiO_2/rGO (1:0.03)	2.93
TiO_2/rGO (1:0.04)	2.89
TiO_2/rGO (1:0.05)	2.92

5.2.1.2 Photoluminescence measurement

Photoluminescence (PL) was employed to investigate the efficiency of charge carrier trapping, immigration and transfer of the photogenerated electrons and holes in photocatalyst. The PL spectra of TiO_2 and TiO_2/rGO catalysts were measured in the wavelength from 375 nm to 550 nm under 325 nm light excitation (as seen in Figure 18). Broad emission band of TiO_2/rGO catalysts were smaller than that of TiO_2. With the increasing amount of rGO, the emission intensity gradually weakened. TiO_2/rGO (1:0.04) exhibited the lowest emission intensity. Therefore, the photogenerated electrons of TiO_2 were effectively transferred to rGO with slower recombination rate, thereby generating more activated •OH for methylene blue degradation. The rGO was added to catalyst in order to decrease the electrons-holes recombination because of its excellent electron transportation properties. Consequently, lower electron-hole recombination endowed the TiO_2/rGO catalyst with high photocatalytic activity.
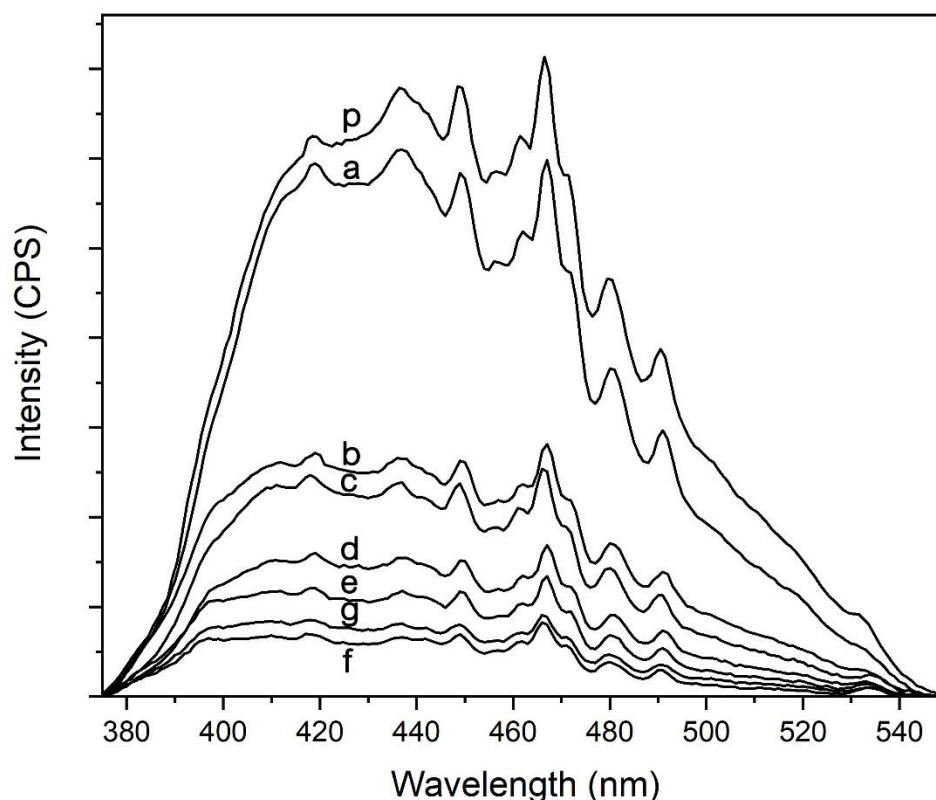
Figure 18 PL spectra of (p) TiO_2, (a) TiO_2/rGO (1:0), (b) TiO_2/rGO (1:0.005), (c) TiO_2/rGO (1:0.01), (d) TiO_2/rGO (1:0.02), (e) TiO_2/rGO (1:0.03), (f) TiO_2/rGO (1:0.04), and (g) TIO_2/rGO (1:0.05)

5.2.1.3 FTIR analysis

The FTIR spectra of TiO_2, APTMS-TiO_2 (22.1 mmol) and TiO_2/rGO catalysts were investigated by Fourier transform infrared spectroscopy with a transmittance mode (As seen in Figure 19). The strong band in the wavenumber range of 550-900 cm^{-1} was assigned to Ti-O-Ti stretching vibration [10] and was observed in every sample. After TiO_2 surface was modified with APTMS, small peaks at 1017 cm^{-1} and 1100 cm^{-1} were detected, were attributed to the stretching vibrations of Si-O-Ti and Si-O-Si, respectively [61]. This signal was a result of a chemical interaction between TiO_2 and APTMS on the surface of modified TiO_2. When rGO was added to the APTMS-TiO_2, the peak at 1017 cm^{-1} and 1100 cm^{-1} became smaller. This result suggested that the rGO sheets were wrapped around APTMS-TiO_2 particles.
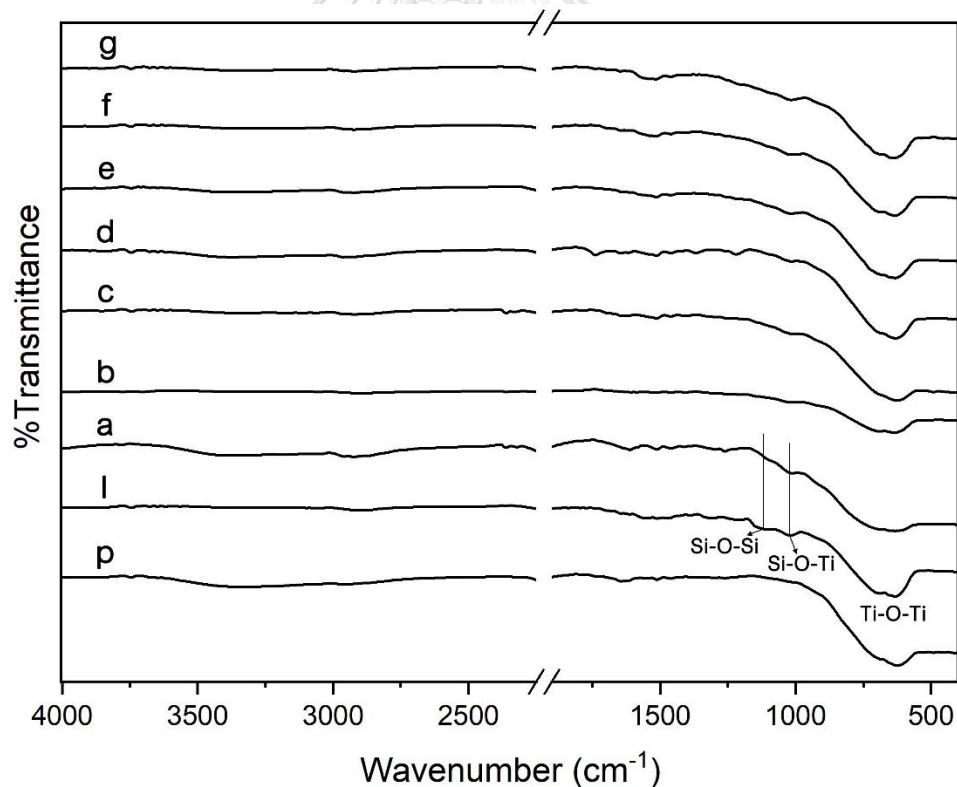
Figure 19 FTIR spectra of (p) TiO_2, (l) APTMS-TiO_2 (22.1 mmol), (a) TiO_2/rGO (1:0),

(b) TiO_2/rGO (1:0.005), (c) TiO_2/rGO (1:0.01), (d) TiO_2/rGO (1:0.02),

(e) TiO_2/rGO (1:0.03), (f) TiO_2/rGO (1:0.04), and (g) TIO_2/rGO (1:0.05)

5.2.1.4 Phase structure

The phase structures of TiO_2 and TiO_2/rGO catalysts were characterized using X-ray diffractometry (XRD). In Figure 20, the diffraction peaks at 2θ of 25.4°, 37.8°, 47.8°, 54.4°, 68.8°, and 75.2° were assigned to the anatase phase. The peaks at 2θ of 27.4°, 36.1°, 41.2°, and 62.8° corresponded to rutile phase and a small peak at 2θ of 30.7° was assigned to brookite phase. Moreover, the XRD pattern of TiO_2/rGO catalysts was similar to TiO_2 and the diffraction peak of rGO was not detected.

The crystallite sizes of TiO_2 and TiO_2/rGO catalyst were calculated by Debye-Scherer equation (in Appendix D). Table 6 listed the crystallite size of TiO_2 and TiO_2/rGO catalysts. The crystallite sizes of TiO_2 and TiO_2/rGO catalysts were almost unchanged (7.4 -7 . 9 nm) because TiO_2 and TiO_2/rGO were calcined only once at the same temperature.

The phase composition of TiO_2 and TiO_2/rGO catalysts was displayed in Table 6. The calculation of phase composition was shown in Appendix E. TiO_2 consisted of 72% anatase, 17% rutile, and 11% brookite. After TiO_2 was wrapped with rGO, the composition of anatase phase was slightly reduced and the composition of rutile phase was slightly increased because anatase phase transformed to rutile phase when being heated during the reflux process [6].
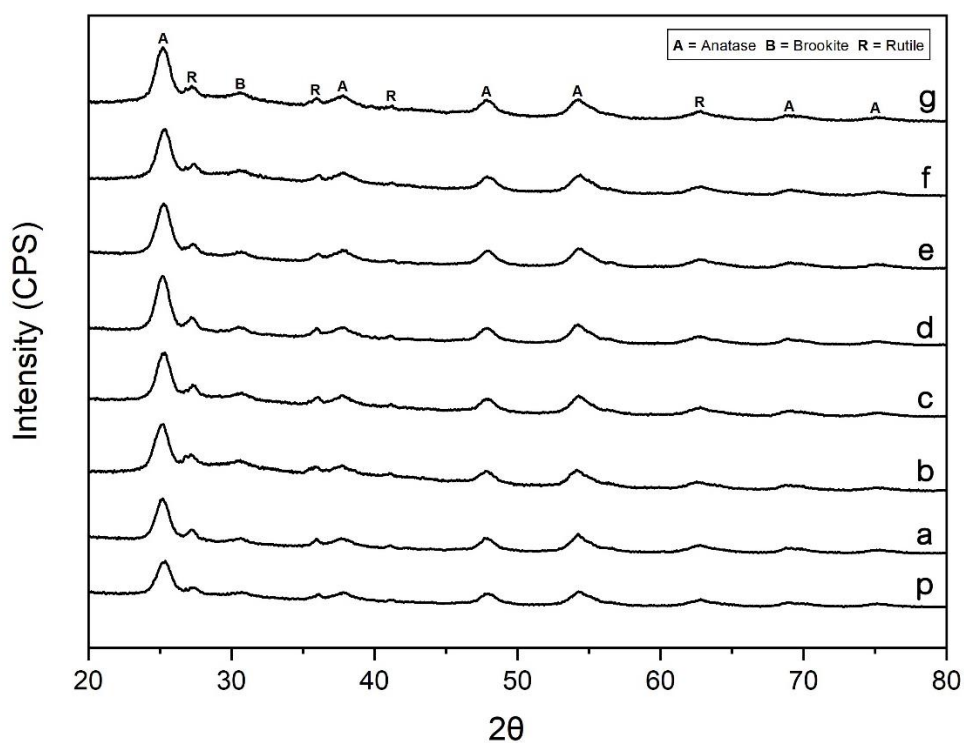
Figure 20 XRD patterns of (p) TiO$_2$, (a) TiO$_2$/rGO (1:0),

(b) TiO$_2$/rGO (1:0.005), (c) TiO$_2$/rGO (1:0.01), (d) TiO$_2$/rGO (1:0.02),

(e) TiO$_2$/rGO (1:0.03), (f) TiO$_2$/rGO (1:0.04), and (g) TIO$_2$/rGO (1:0.05)

Table 6 Crystallite size and phase composition of TiO$_2$ and TiO$_2$/rGO catalysts

Sample	Crystallite size (nm)	Phase composition (%)		
		Anatase	Rutile	Brookite
TiO$_2$	7.7	72	17	11
TiO$_2$/rGO (1:0)	7.8	67	22	11
TiO$_2$/rGO (1:0.005)	7.8	65	21	14
TiO$_2$/rGO (1:0.01)	7.9	64	22	13
TiO$_2$/rGO (1:0.02)	7.9	65	22	13
TiO$_2$/rGO (1:0.03)	7.6	70	17	13
TiO$_2$/rGO (1:0.04)	7.9	67	19	14
TiO$_2$/rGO (1:0.05)	7.4	67	20	14

5.2.1.5 Measurement of specific surface area

The specific surface areas of TiO_2, rGO, and TiO_2/rGO catalysts are listed in Table 7. TiO_2 had a specific surface area of 108.2 m^2/g. When rGO was added to TiO_2/rGO catalysts, the surface area of TiO_2/rGO catalysts increased to 104.9-119.3 m^2/g. An increase in specific surface areas came from rGO that had has a high specific surface area (295.9 m^2/g).

Table 7 Surface area of TiO_2, rGO, and TiO_2/rGO catalysts

Sample	Surface area (m^2/g)
TiO_2	108.2
rGO	295.9
TiO_2/rGO (1:0)	94.4
TiO_2/rGO (1:0.005)	104.9
TiO_2/rGO (1:0.01)	107.2
TiO_2/rGO (1:0.02)	109.5
TiO_2/rGO (1:0.03)	114.8
TiO_2/rGO (1:0.04)	119.3
TiO_2/rGO (1:0.05)	116.2

5.2.1.6 Morphological features

The SEM images were used to confirm that rGO wrapped around the surface of APTMS-TiO$_2$ (22.1 mmol). The morphology of rGO, APTMS-TiO$_2$ (22.1 mmol), and TiO$_2$/rGO catalyst were displayed in Figure 21. The rGO sheets possessed rough and corrugated texture (see Figure 21(a)). From Figure 21(b), one saw TiO$_2$ spherical particles. After APTMS modification, the morphology of APTMS-TiO$_2$ was similar to that of TiO$_2$ as shown in Figure 21(c). Figure 21(d) displayed a group of TiO$_2$ spherical particles that are wrapped with rGO sheets, suggesting the successful wrapping of rGO.
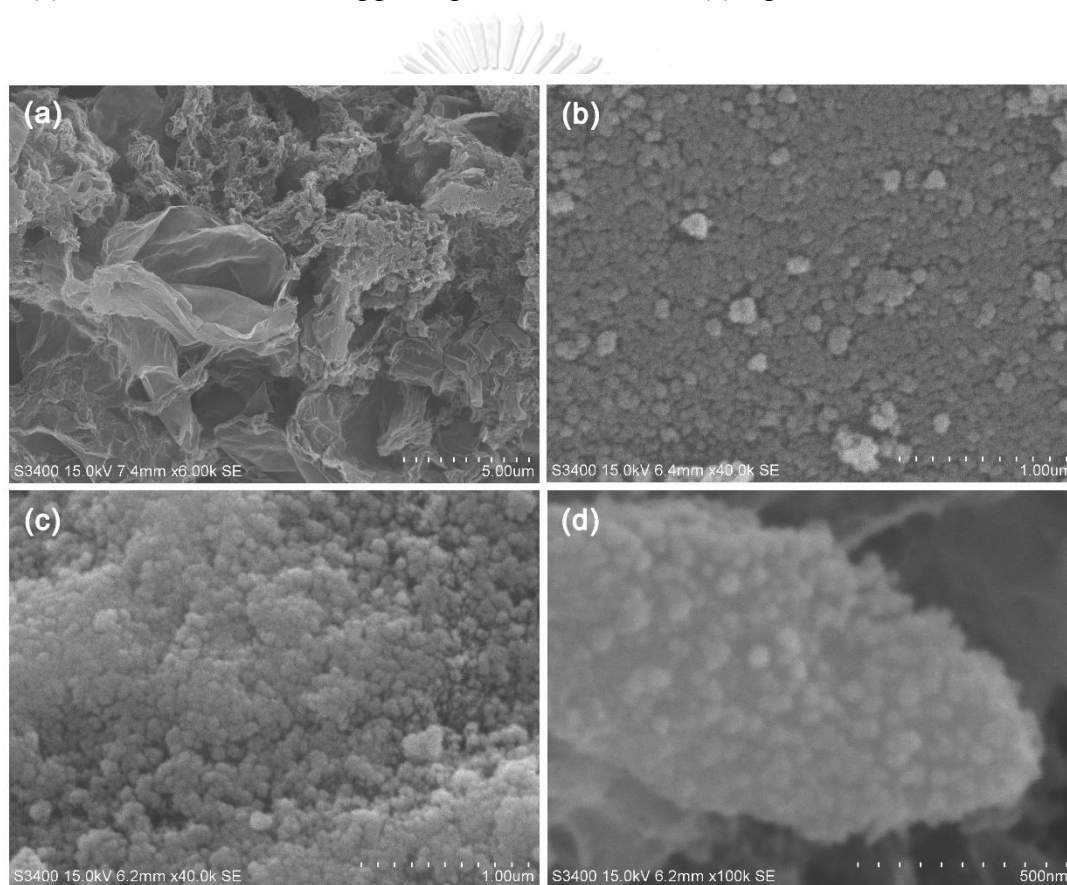
Figure 21 SEM image (magnification: 6k) of (a) rGO

SEM images (magnification: 40k) of (b) TiO$_2$, (c) APTMS-TiO$_2$ (22.1 mmol).

SEM image (magnification: 40k) of (d) TiO$_2$/rGO

5.2.2 Photocatalytic performance

The photocatalytic performance of TiO_2 and TiO_2/rGO catalysts were evaluated in photocatalytic degradation of methylene blue under UV and visible light irradiations. The catalyst was put in a methylene blue solution and the mixture was stirred constantly in the dark for 1 hour to achieve adsorption equilibrium. After that, the mixture was exposed to either UV or visible light for 3 hours. The sample was collected every 15 minutes to determine the conversion of methylene blue in the photocatalytic reaction.

5.2.2.1 The degradation under UV light irradiation over TiO_2 and TiO_2/rGO catalysts

The photocatalytic activities of TiO_2 and TiO_2/rGO catalysts were investigated for the degradation of methylene blue under UV irradiation as shown in Figure 22. In Table 8, the experiment without catalyst produced the lowest conversion. At the beginning of the experiment (t=0), The initial concentration of methylene blue in the solution that contained TiO_2/rGO catalysts were lower than that with TiO_2 because the higher specific surface area of TiO_2/rGO catalysts possibly adsorbed more dye. An increasing amount of rGO in the catalyst produced higher conversion of methylene blue than TiO_2 did. Thus, addition of rGO enhanced the photocatalytic activity. The highest conversion was observed for TiO_2/rGO (1:0.04) because of the reduced electron-hole recombination (see Figure 18), and better visible light absorption (see Figure 16).
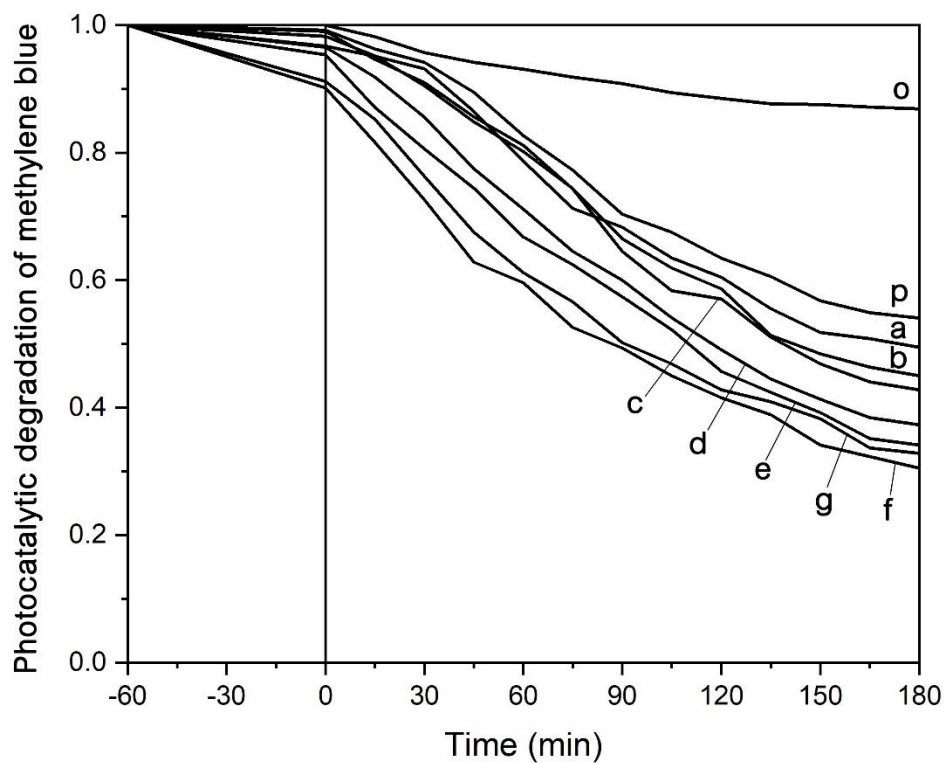
Figure 22 Photocatalytic degradation of methylene blue result under UV light

irradiations using (o) no catalyst, (p) TiO$_2$, (a) TiO$_2$/rGO (1:0),

(b) TiO$_2$/rGO (1:0.005), (c) TiO$_2$/rGO (1:0.01), (d) TiO$_2$/rGO (1:0.02),

(e) TiO$_2$/rGO (1:0.03), (f) TiO$_2$/rGO (1:0.04), and (g) TIO$_2$/rGO (1:0.05)

จุฬาลงกรณ์มหาวิทยาลัย

CHULALONGKORN UNIVERSITY

Table 8 The conversion of methylene blue degradation after 3 hours of UV light exposure over TiO_2 and TiO_2/rGO catalysts

Sample	Conversion
no catalyst	13.13
TiO_2	45.93
TiO_2/rGO (1:0)	50.51
TiO_2/rGO (1:0.005)	55.00
TiO_2/rGO (1:0.01)	57.17
TiO_2/rGO (1:0.02)	62.72
TiO_2/rGO (1:0.03)	65.87
TiO_2/rGO (1:0.04)	69.47
TiO_2/rGO (1:0.05)	67.19

5.2.2.2 The degradation under visible light irradiation over TiO_2 and TiO_2/rGO catalysts

The photocatalytic activity of TiO_2 and TiO_2/rGO catalysts were evaluated by the degradation of methylene blue under visible irradiation as seen in Figure 23. The order of increasing photocatalytic activity was TiO_2, TiO_2/rGO (1:0), TiO_2/rGO (1:0.005), TiO_2/rGO (1:0.01), TiO_2/rGO (1:0.02), TiO_2/rGO (1:0.03), TiO_2/rGO (1:0.05) and TiO_2/rGO (1:0.04). This same trend was observed in the results of PL, UV-vis, and bandgap values. Similar to the experiments under UV irradiation, the highest conversion was observed for TiO_2/rGO (1:0.04) (see Table 9). The optimum value of rGO content in APTMS-TiO_2 for degradation of methylene blue is 4 %wt. Obviously, the photocatalytic activity of the catalyst under UV irradiation was higher than that of the catalyst under visible irradiation because UV irradiation consisted of photon with higher energy than visible irradiation did, leading to generation of more •OH, which decomposed methylene blue.
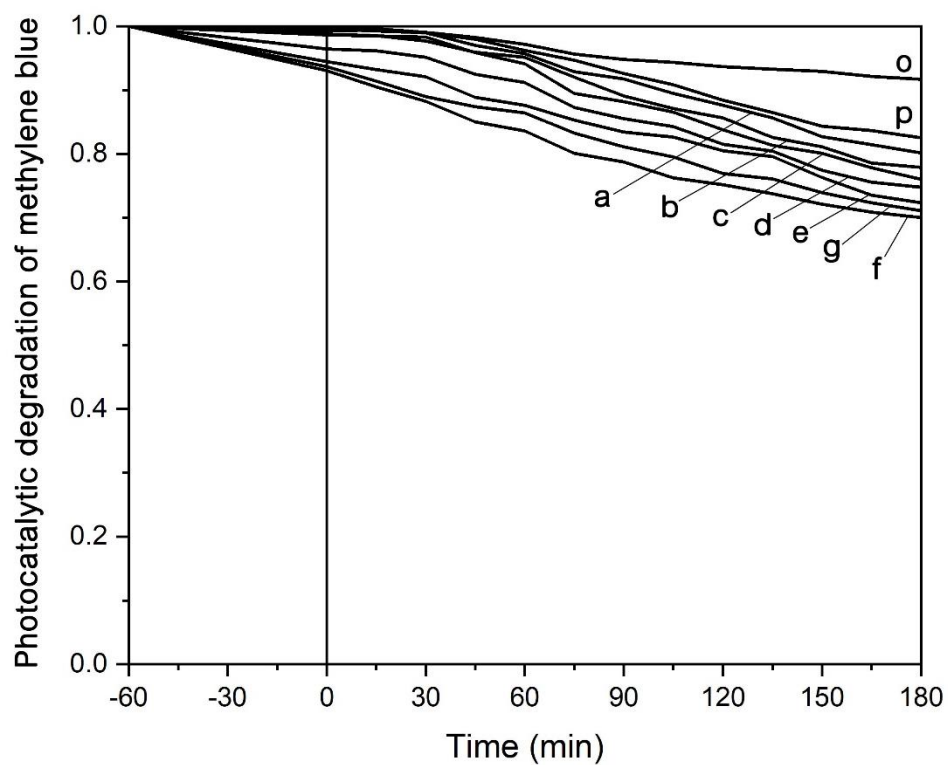
Figure 23 Photocatalytic degradation of methylene blue result under visible light

irradiations using (o) no catalyst, (p) TiO_2, (a) TiO_2/rGO (1:0), (a) TiO_2/rGO (1:0),

(b) TiO_2/rGO (1:0.005), (c) TiO_2/rGO (1:0.01), (d) TiO_2/rGO (1:0.02),

(e) TiO_2/rGO (1:0.03), (f) TiO_2/rGO (1:0.04), and (g) TIO_2/rGO (1:0.05)

Table 9 The conversion of methylene blue degradation under visible light over TiO_2 and TiO_2/rGO catalysts

Sample	Conversion
no catalyst	8.31
TiO_2	17.47
TiO_2 /rGO (1:0)	19.87
TiO_2 /rGO (1:0.005)	22.13
TiO_2 /rGO (1:0.01)	23.96
TiO_2 /rGO (1:0.02)	25.23
TiO_2 /rGO (1:0.03)	27.67
TiO_2 /rGO (1:0.04)	29.96
TiO_2 /rGO (1:0.05)	28.91

CHAPTER 5.3

RESULTS AND DISCUSSION

OF SURFACE MODIFICATION OF CATALYSTS

WITH AMOUNT OF APTMS

The results and discussion in chapter 5.3 investigated the effect of varying the amount of APTMS between 2.21 and 22.1 mmol in catalyst. In the surface modification of TiO_2 with APTMS, the amount of APTMS was reduced from 22.1 mmol to 2.21 mmol because the thin layer of APTMS exhibited higher photocatalytic activity than the thick layer of APTMS [35]. TiO_2/rGO catalysts were synthesized from APTMS-TiO_2 (22.1 mmol) and were wrapped with rGO, while TiO_2/rGO* catalysts were synthesized from APTMS-TiO_2 (2.21 mmol) and were wrapped with rGO.   This chapter are divided into two major parts. In the first part, the results from several characterization techniques for the TiO_2/rGO and TiO_2/rGO* catalysts including UV-vis, PL, FTIR, XRD, N_2 physisorption, and SEM are described. And in the second part, the photocatalytic degradation of methylene blue in UV and visible irradiation was discussed. This chapter we selected the amount of rGO in the catalyst to be 0, 0.02, and 0.04 g because TiO_2/rGO (1:0.04) gave the best catalytic performance in Chapter 5.2.

5.3.1 Characterization of the APTMS-TiO_2 and TiO_2/rGO* catalysts

5.3.1.1 TGA analysis

There were three stages of weight loss as seen in Figure 24. The first stage, weight loss below at 120 °C was caused by water elimination from surface and pore. The second stage, weight loss at the range of 120-300 ° C corresponded to the removal of chemisorbed hydroxyl group [35]. The last stage, weight loss at the range of 300-550 ° C was a result of amine group decomposition [62, 63]. In addition, the weight loss of APTMS-TiO_2 (Figure 24(k)&(l)) was smaller than that of TiO_2 (Figure 24(p)) in the temperature range of 120-300 ° C, indicating that APTMS-TiO_2 had a lower moisture content than TiO_2 had due to the hydrophobic property of Si-O-Si group [64]. The amine content of APTMS-

TiO_2 (22.1 mmol) was greater than APTMS-TiO_2 (2.21 mmol) so its total weight loss was larger than APTMS-TiO_2 (2.21 mmol). Thus, the total weight loss of 3.82 %wt, 8.35 %wt and 13.38 %wt for TiO_2, APTMS-TiO_2 (2.21 mmol), and APTMS-TiO_2 (22.1 mmol) respectively.
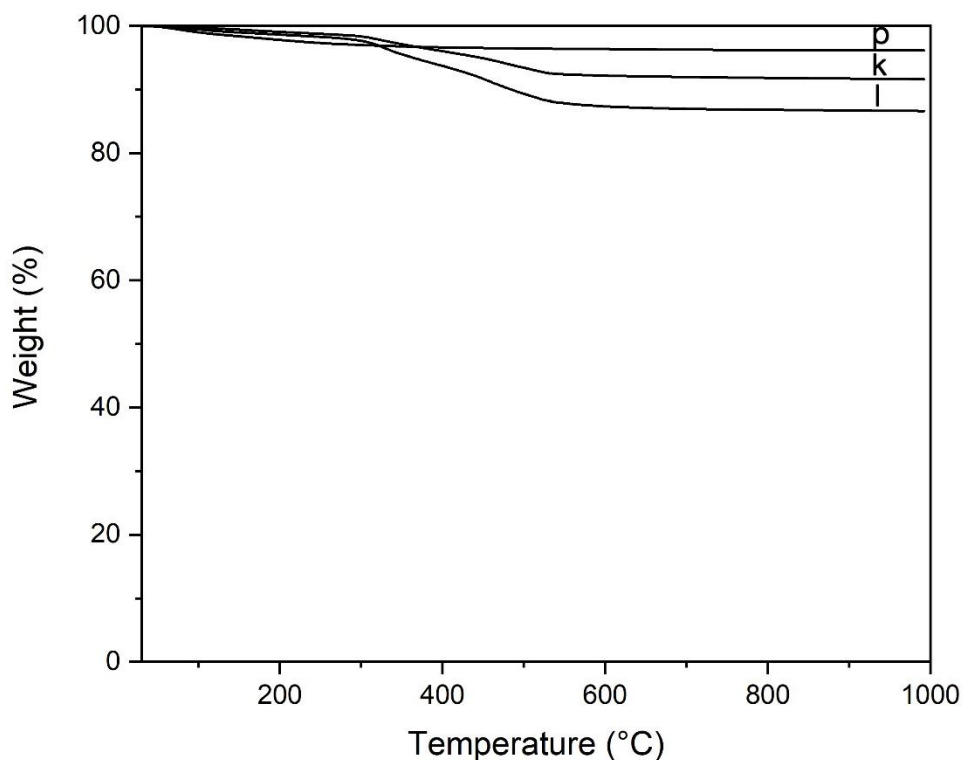
Figure 24 TGA of (p) TiO_2, (k) APTMS-TiO_2 (2.21 mmol),
and (l) APTMS-TiO_2 (22.1 mmol)

5.3.1.2 Optical absorption properties

To compare the optical absorption properties of TiO_2/rGO and TiO_2/rGO* catalysts, we selected the TiO_2/rGO and TiO_2/rGO* catalysts that contained the same amount of rGO (see Figure 25). The modification of the surface of TiO_2 with APTMS enhanced the optical absorption properties [65]. TiO_2/rGO* catalyst had better absorption than TiO_2/rGO catalyst had because the thin layer of N and Si from APTMS on TiO_2 surface was better at promoting the absorption than thick layer of N and Si [66-69]. Therefore, reducing the amount of APTMS gave rise to better absorption [38].
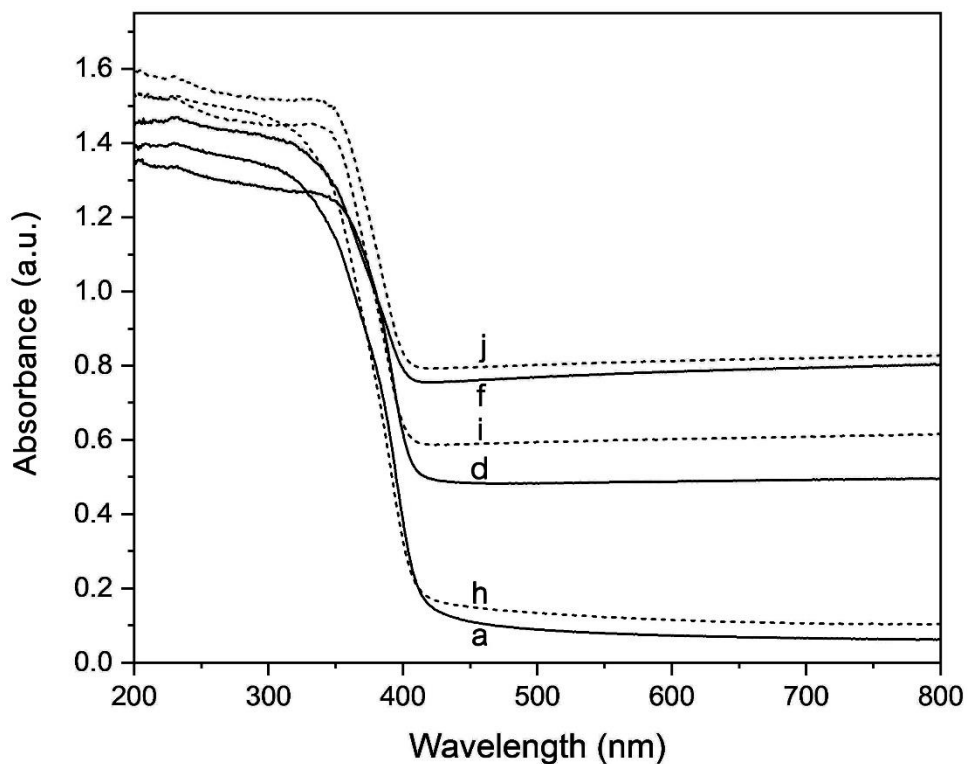
Figure 25 UV–Vis spectra of (a) TiO_2/rGO (1:0), (h) TiO_2/rGO (1:0)*, (d) TiO_2/rGO (1:0.02), (i) TiO_2/rGO (1:0.02)*, (f) TiO_2/rGO (1:0.04), and (j) TiO_2/rGO (1:0.04)*

In addition, the bandgap of samples was calculated using the information from Figure 25. The plot in Figure 26 was prepared and the calculated bandgap was listed in Table 10. TiO_2/rGO* catalyst (modified surface with APTMS 2.21 mmol) possessed slightly smaller bandgap than TiO_2/rGO catalyst (modified surface with APTMS 22.1 mmol) did. The narrow bandgap resulted in electrons moving from the valence band to the conduction band more easily and quickly than the wider bandgap. The N and Si created the intermediate states within TiO_2 bandgap, leading to narrowing bandgap [67, 68]. Therefore, a thin layer of N and Si on TiO_2 surface also improved the light absorption [66-69].
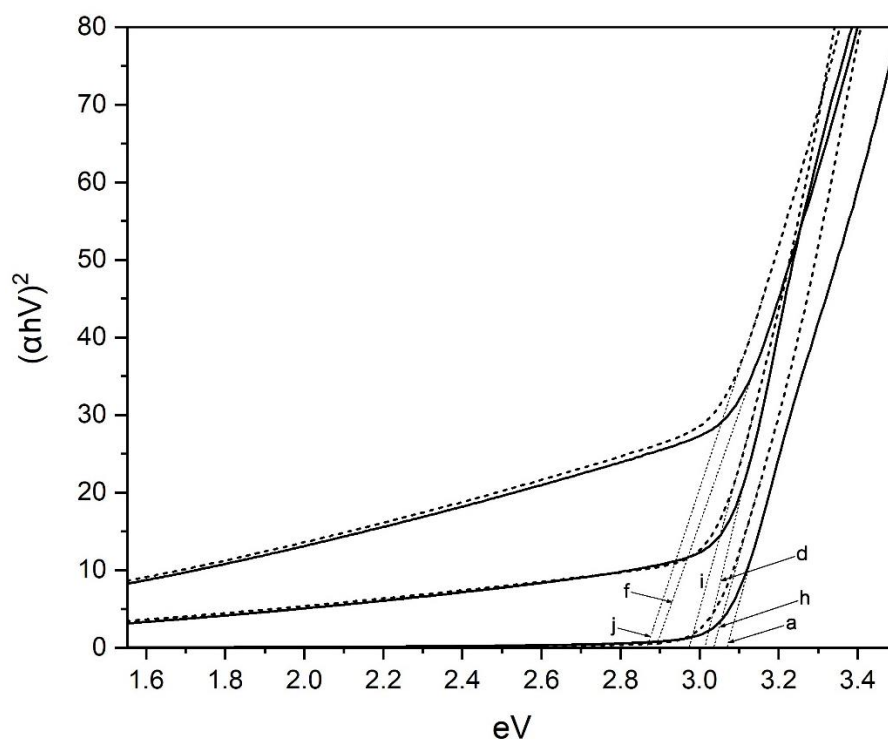
Figure 26 Plot of the bandgap, as derived from the diffuse reflectance UV–Vis spectra of (a) TiO_2/rGO (1:0), (h) TiO_2/rGO (1:0)*, (d) TiO_2/rGO (1:0.02), (i) TiO_2/rGO (1:0.02)*, (f) TiO_2/rGO (1:0.04), and (j) TiO_2/rGO (1:0.04)*

Table 10 The comparison bandgap from UV-vis spectra of APTMS-TiO_2 and TiO_2/rGO* catalysts

Sample	Bandgap (eV)
TiO_2/rGO (1:0)	3.06
TiO_2/rGO (1:0.02)	2.99
TiO_2/rGO (1:0.04)	2.89
TiO_2/rGO (1:0)*	3.03
TiO_2/rGO (1:0.02)*	2.96
TiO_2/rGO (1:0.04)*	2.86

5.3.1.3 Photoluminescence measurement

The PL spectra of TiO_2/rGO and TiO_2/rGO* catalysts were compared in Figure 27. The low intensity of PL was ascribed to slower rate of recombination of the charge carriers. The emission band at 375-550 nm was attributed to the emission from the electron-hole recombination. The PL spectra of samples were obtained using an excitation wavelength of 325 nm. As a result, the APTMS-TiO_2 revealed a spectrum with lower intensity than that of TiO_2 [70]. With the same rGO content, TiO_2/rGO* catalyst (using APTMS 2.21 mmol) exhibited lower emission intensity than TiO_2/rGO catalyst (using APTMS 22.1 mmol). This is an evidence that the thin layer of N and Si coverage on TiO_2 surface reduced the recombination rate of electron and hole [71, 72]. Hence, TiO_2/rGO* catalyst can slightly enhance the photocatalytic activity.
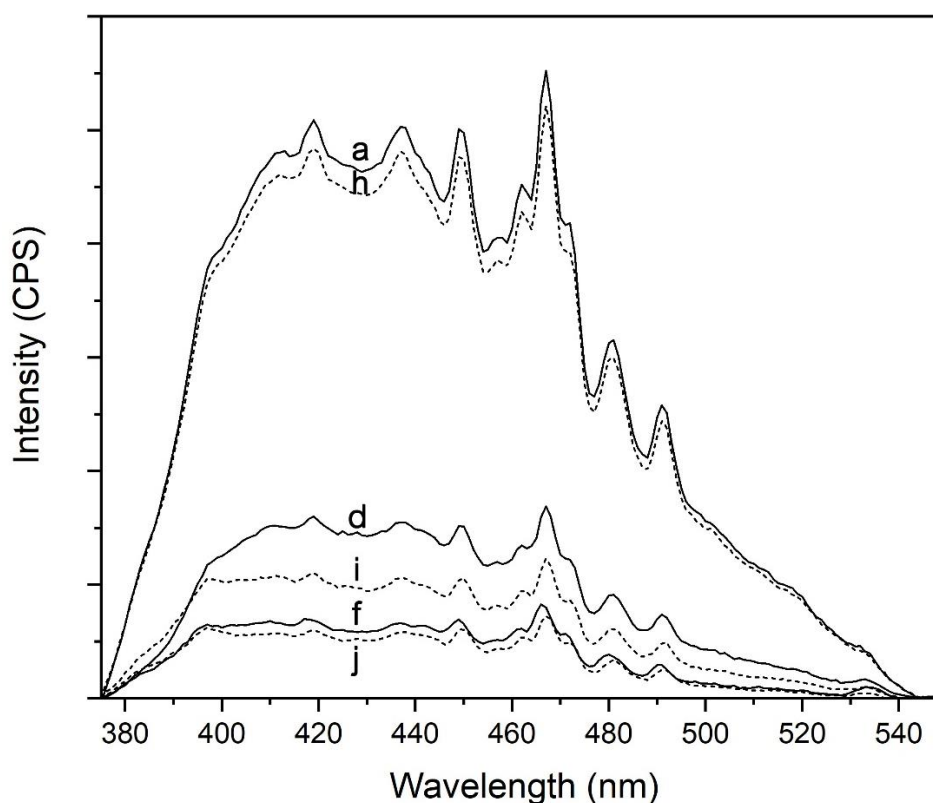
Figure 27 PL spectra of (a) TiO_2/rGO (1:0), (h) TiO_2/rGO (1:0)*, (d) TiO_2/rGO (1:0.02), (i) TiO_2/rGO (1:0.02)*,(f) TiO_2/rGO (1:0.04), and (j) TiO_2/rGO (1:0.04)*

5.3.1.4 FTIR analysis

The FTIR spectra of APTMS-TiO$_2$ (2.21 mmol), APTMS-TiO$_2$ (22.1mmol), TiO$_2$/rGO, and TiO$_2$/rGO* catalysts were displayed in Figure 28. Intensive bands at wavenumbers of 600-710 cm^{-1} were clearly observed. These bands were related to the stretching of Ti-O-Ti bonds [10]. After the modification using APTMS 22.1 mmol, two small peaks appeared at 1017 cm^{-1} and, 1100 cm^{-1}. They were attributed to the vibrations of Si-O-Ti, Si-O-Si [61], But when APTMS 2.21 mmol was used, instead of 22.1 mmol, both peaks became smaller. The Si-O-Ti bond in the APTMS-TiO$_2$ was created from the reaction between caused by methoxy groups (CH$_3$O-R) of APTMS and hydroxyl groups on the TiO$_2$ surface (Ti-OH). Therefore, varying the amount of APTMS affected the surface properties of TiO$_2$ (as seen in Figure 28 (l)-(k)). In comparison, FTIR spectra of TiO$_2$/rGO and TiO$_2$/rGO* appeared similar (as seen in Figure 28(a,d,f,h,l,j)).
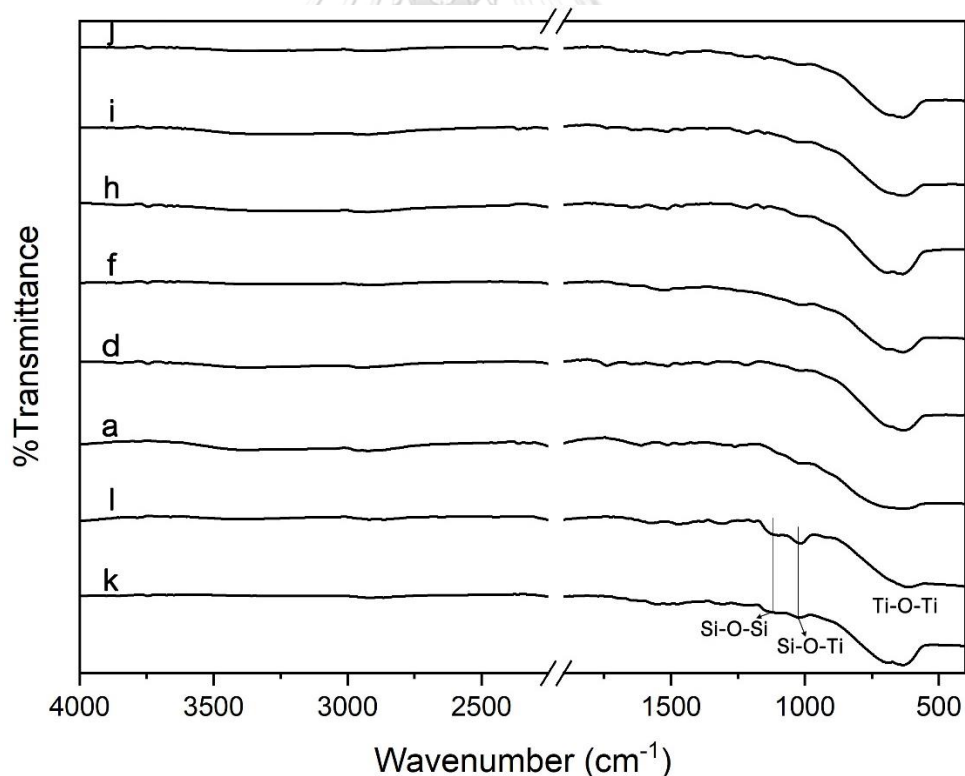
Figure 28 FTIR spectra of (k) APTMS-TiO$_2$ (2.21 mmol), (l) APTMS-TiO$_2$ (22.1 mmol),
(a) TiO$_2$/rGO (1:0), (d) TiO$_2$/rGO (1:0.02), (f) TiO$_2$/rGO (1:0.04), (h) TiO$_2$/rGO (1:0)*,
(i) TiO$_2$/rGO (1:0.02)*, and (j) TiO$_2$/rGO (1:0.04)*

5.3.1.5 Phase structure

The phase structure of APTMS-TiO$_2$, TiO$_2$/rGO, and TiO$_2$/rGO* catalysts were determined from XRD results (see in Figure 29). The XRD peaks detected at 2θ of 25.4°, 37.8°, 47.8°, 54.4°, 68.8°, and 75.2° corresponded to anatase phase. The diffraction peaks at 2θ of 27.4°, 36.1°, 41.2°, and 62.8° were assigned to rutile phase and brookite phase occurred at 2θ of 30.7°. The XRD patterns of APTMS-TiO$_2$ (2.21 mmol), TiO$_2$/rGO, and TiO$_2$/rGO* catalysts appeared similar. In Figure 29(l), the excessive amount of amine coating on TiO$_2$ lowered the diffraction peak intensity. APTMS-TiO$_2$ (22.1 mmol) was wrapped with rGO through the similar reflux process, resulting in the intensity of TiO$_2$/rGO in XRD pattern resembling the intensity of TiO$_2$/rGO* in XRD pattern [10, 73] because some APTMS was removed during the reflux process [45].

Calculation of crystallites size was demonstrated in Appendix D. The crystallites size of APTMS-TiO$_2$, TiO$_2$/rGO, and TiO$_2$/rGO* catalysts were in the range 7.6-7.9 nm as seen in Table 11. A change in crystallite size was hardly detectable because the temperature of the reflux process during rGO wrapping was too low to give rise to the sintering of TiO$_2$ [74].

Determination of phase composition was shown in Appendix E. Table 11 shows the phase composition of the APTMS-TiO$_2$, TiO$_2$/rGO, and TiO$_2$/rGO* catalysts. When comparing the phase composition among the catalysts, the phase composition of APTMS-TiO$_2$, TiO$_2$/rGO, and TiO$_2$/rGO catalysts did not change that much because they underwent the same process.
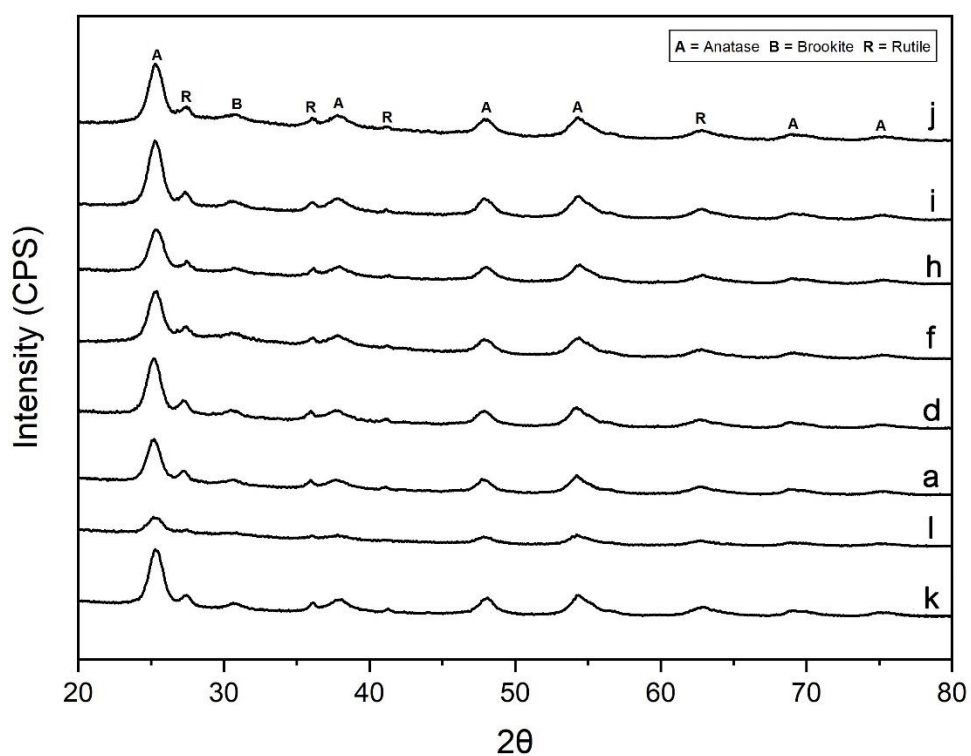
Figure 29 XRD patterns of (k) APTMS-TiO$_2$ (2.21 mmol), (l) APTMS-TiO$_2$ (22.1 mmol),

(a) TiO$_2$/rGO (1:0), (d) TiO$_2$/rGO (1:0.02), (f) TiO$_2$/rGO (1:0.04), (h) TiO$_2$/rGO (1:0)*,

(i) TiO$_2$/rGO (1:0.02)*, and (j) TiO$_2$/rGO (1:0.04)*

Table 11 Crystallite size and Phase composition of APTMS-TiO$_2$, TiO$_2$/rGO and

TiO$_2$/rGO* catalysts

Sample	Crystallite size (nm)	Phase composition (%)		
		Anatase	Rutile	Brookite
APTMS-TiO$_2$ (2.21 mmol)	7.8	70	19	10
APTMS-TiO$_2$ (22.1 mmol)	7.5	66	20	14
TiO$_2$/rGO (1:0)	7.8	67	22	11
TiO$_2$/rGO (1:0.02)	7.9	65	22	13
TiO$_2$/rGO (1:0.04)	7.9	67	19	14
TiO$_2$/rGO (1:0)*	7.6	67	22	11
TiO$_2$/rGO (1:0.02)*	7.8	69	20	11
TiO$_2$/rGO (1:0.04)*	7.6	69	19	11

5.3.1.6 Measurement of specific surface area

The specific surface areas of TiO_2, APTMS-TiO_2, TiO_2/rGO, and TiO_2/rGO* catalysts along with the pore volumes of TiO_2, APTMS-TiO_2 are listed in Table 12. After modifiying TiO_2 surface with APTMS, the specific surface area and pore volume of the APTMS-TiO_2 dropped significantly, because APTMS entered the pore of TiO_2, leading to pore blockage [62]. This result was evidenced by the decrease in pore volume with an increasing amine content. From Table 12, TiO_2/rGO* catalyst possessed a larger surface area than TiO_2/rGO catalyst did because TiO_2/rGO* catalyst employed APTMS 2.21 mmol 10 times lower than that used in TiO_2/rGO catalyst, causing less pore blockage.

Table 12 Specific surface areas of TiO_2, APTMS-TiO_2, TiO_2/rGO, and TiO_2/rGO* catalysts and pore volumes of TiO_2, and APTMS-TIO_2

Sample	Surface area (m^2/g)	Pore volume (cm^3/g)
TiO_2	108.2	0.248
APTMS-TiO_2 (2.21 mmol)	89.1	0.147
APTMS-TiO_2 (22.1 mmol)	28.5	0.034
TiO_2/rGO (1:0)	94.4	-
TiO_2/rGO (1:0.02)	109.5	-
TiO_2/rGO (1:0.04)	119.3	-
TiO_2/rGO (1:0)*	105.8	-
TiO_2/rGO (1:0.02)*	116.3	-
TiO_2/rGO (1:0.04)*	124.7	-

5.3.1.7 Morphological features

The SEM images shows the morphology of the catalysts that was modified with a different amount of APTMS (see Figure 30). Figures 30 (a) and (b) displayed the morphology of TiO_2 surface modified using 2.21 and 22.1 mmol of APTMS, respectively.

The morphology of APTMS-TiO$_2$ (2.21 mmol) and APTMS-TiO$_2$ (22.1 mmol) appeared similarly as spherical particles. Modified surface of TiO$_2$ with APTMS was not changing the morphology. Figure 30 (c) and (d) showed the APTMS-TiO$_2$ catalysts that were wrapped with rGO. Both of them also looked similar.
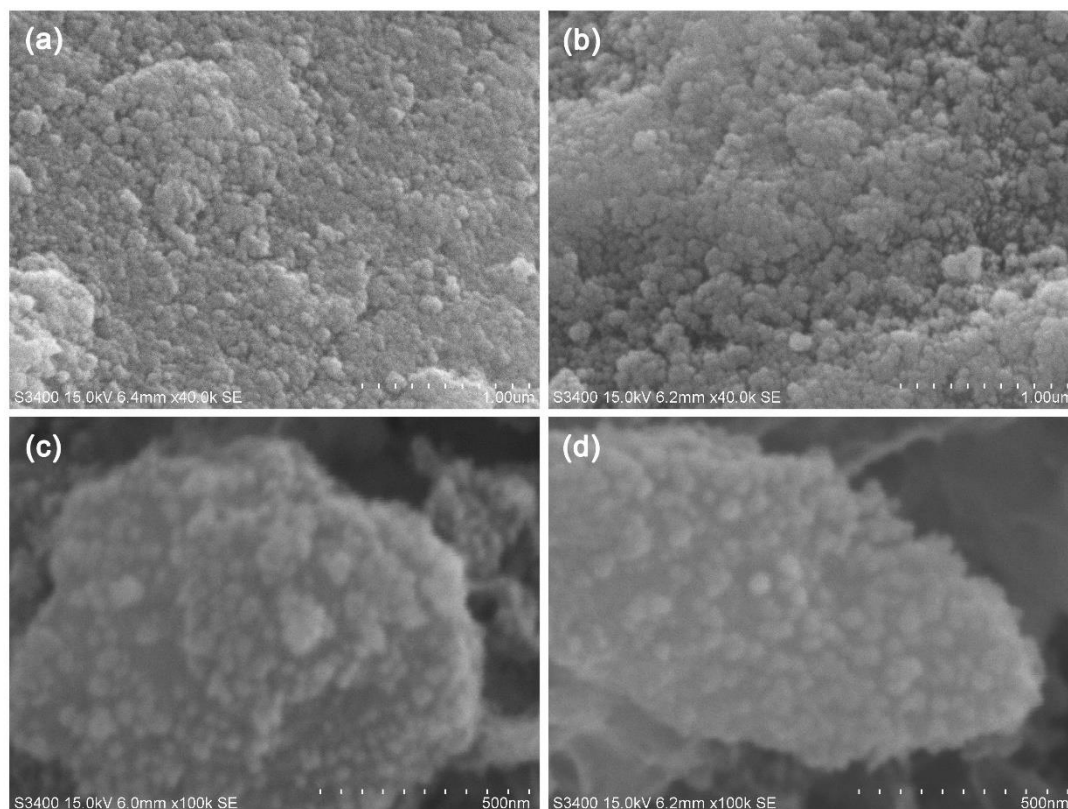
Figure 30 SEM images (magnification: 40k) of (a) APTMS-TiO$_2$ (2.21 mmol), (b) APTMS-TiO$_2$ (22.1 mmol) and SEM images (magnification: 100k) of (c) TiO$_2$/rGO (1:0.04)*, (d) TiO$_2$/rGO (1:0.04)

5.3.2 Photocatalytic performance

To assess the photocatalytic activities of the TiO$_2$/rGO and TiO$_2$/rGO* catalyst, we investigate the degradation of methylene blue. The system was stirred constantly and was kept in the dark for 1 hour to attain adsorption equilibrium. UV or visible light bulbs were turned on for 3 hours after that and sample was collected every 15 minutes. The concentration of the methylene blue was measured by a UV-Vis spectrophotometer.

5.3.2.1 The degradation under UV light irradiation over TiO_2/rGO and TiO_2/rGO*

catalysts

Figure 31 showed the photocatalytic activity of TiO_2/rGO and TiO_2/rGO* catalysts for the degradation of methylene blue under UV irradiation. When APTMS content was reduced, the conversion of photocatalytic degradation was slightly increased (as seen in Table 13). The order of increasing photocatalytic activities of the catalysts under UV irradiation was TiO_2/rGO (1:0), TiO_2/rGO (1:0)*, TiO_2/rGO (1:0.02), TiO_2/rGO (1:0.02)*, TiO_2/rGO (1:0.04) and TiO_2/rGO (1:0.04)*, respectively. These results were consistent with decline in photoluminescence signals (see Figure 27), better visible light absorption (see Figure 25), and narrowing bandgap (see Figure 26). The results of methylene blue degradation using catalysts under UV light was greater photocatalytic activities than visible lights because UV light comprised photons with higher energy than visible light. As a result, modifying the surface of TiO_2 with APTMS (2.21 mmol) exhibited higher photocatalytic activity than modifying the surface of TiO_2 with APTMS (22.1 mmol). Therefore, TiO_2/rGO (1:0.04)* catalyst exhibited the best performance among all samples.
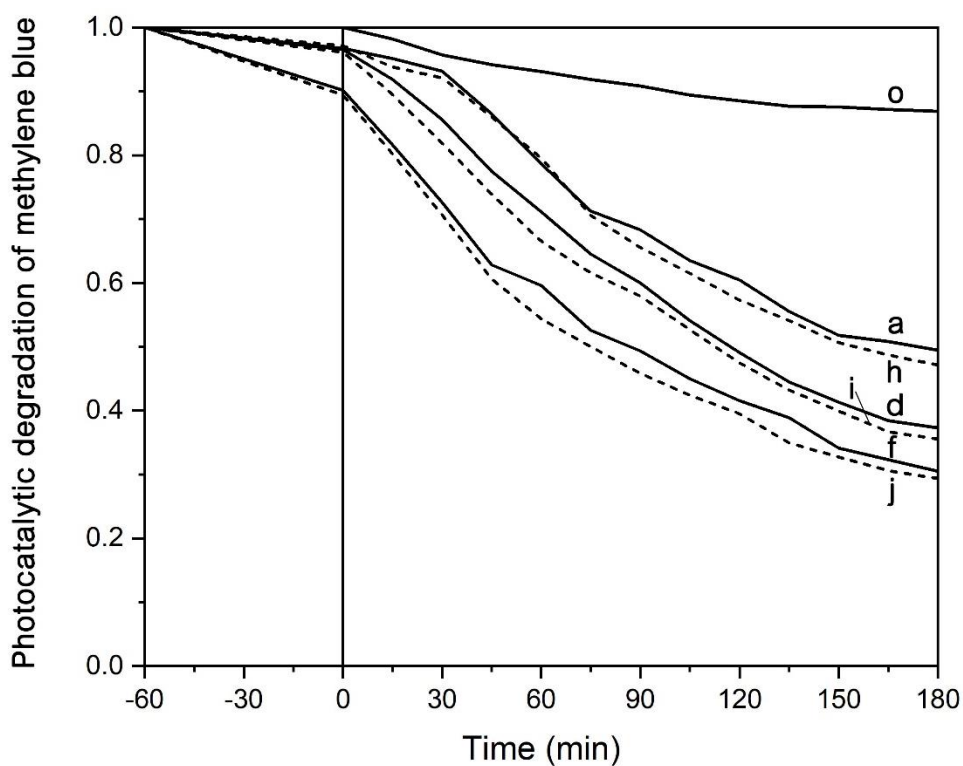
Figure 31 Photocatalytic degradation of methylene blue result under UV light of

(a) TiO$_2$/rGO (1:0), (h) TiO$_2$/rGO (1:0)*, (d) TiO$_2$/rGO (1:0.02),

(i) TiO$_2$/rGO (1:0.02)*,(f) TiO$_2$/rGO (1:0.04), and (j) TiO$_2$/rGO (1:0.04)*

Table 13 The conversion of methylene blue degradation under UV light over TiO$_2$/rGO

and TiO$_2$/rGO* catalysts

Sample	Conversion
no catalyst	13.13
TiO$_2$	45.93
TiO$_2$/rGO (1:0)	50.51
TiO$_2$/rGO (1:0.02)	62.72
TiO$_2$/rGO (1:0.04)	69.47
TiO$_2$/rGO (1:0)*	52.85
TiO$_2$/rGO (1:0.02)*	64.45
TiO$_2$/rGO (1:0.04)*	70.63

5.3.2.2 The degradation under visible light irradiation over TiO_2/rGO and TiO_2/rGO* catalysts

Figure 32 displayed the photocatalytic activity of TiO_2/rGO and TiO_2/rGO* catalysts for the degradation of methylene blue under visible irradiation. This result indicated that modified the surface of TiO_2 with APTMS (2.21 mmol) gave exhibited higher photocatalytic activity than modifying the surface of TiO_2 with APTMS (22.1 mmol). The conversion of methylene degradation was listed in Table 14. It can be seen that TiO_2/rGO (1:0.04)* showed the highest conversion than among all samples. The sequence of photocatalytic activity was consistent with results with decline in photoluminescence signals (see Figure 27), better visible light absorption (see Figure 25), and narrowing bandgap (see Figure 26). However, the photodegradation of methylene blue under visible light was lower conversion than that of the catalyst under UV irradiation because visible irradiation consisted of photon with lower energy than UV irradiation did so electrons in the valence band were less excited to the conduction band, resulting in less •OH.
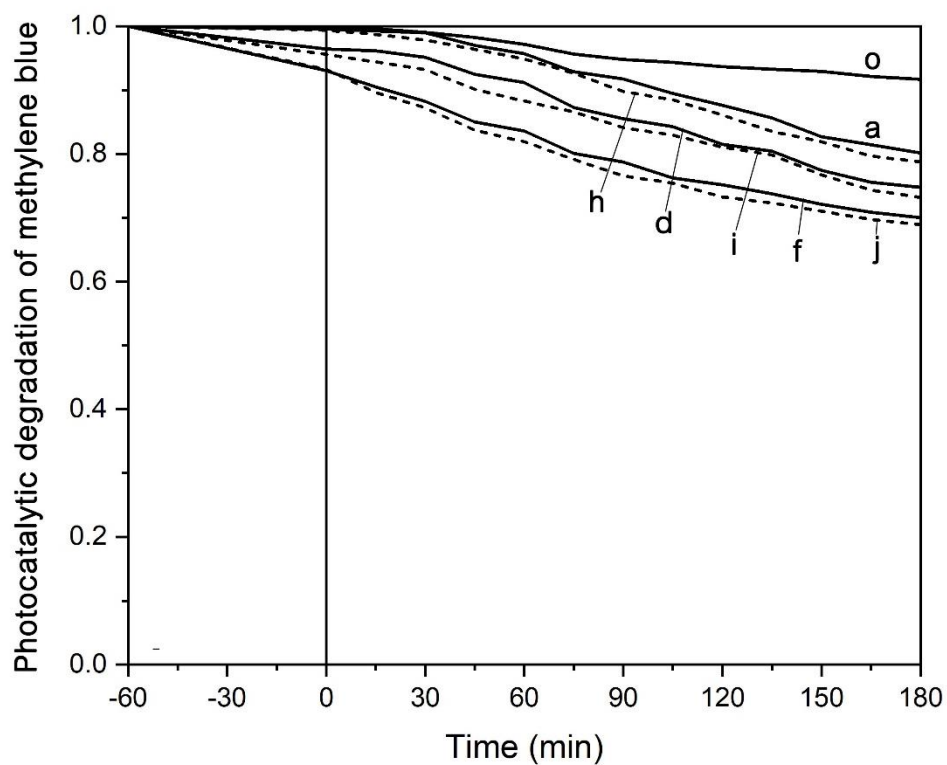
Figure 32 Photocatalytic degradation of methylene blue result under visible light of
(a) TiO$_2$/rGO (1:0), (h) TiO$_2$/rGO (1:0)*, (d) TiO$_2$/rGO (1:0.02),
(i) TiO$_2$/rGO (1:0.02)*,(f) TiO$_2$/rGO (1:0.04), and (j) TiO$_2$/rGO (1:0.04)*

Table 14 The conversion of methylene blue degradation under visible light over TiO$_2$/rGO
and TiO$_2$/rGO* catalysts

Sample	Conversion
no catalyst	8.31
TiO$_2$	17.47
TiO$_2$/rGO (1:0)	19.87
TiO$_2$/rGO (1:0.02)	25.23
TiO$_2$/rGO (1:0.04)	29.96
TiO$_2$/rGO (1:0)*	21.25
TiO$_2$/rGO (1:0.02)*	26.79
TiO$_2$/rGO (1:0.04)*	31.06

CHAPTER 6

CONCLUSIONS AND SUGGESTTION

This chapter is divided into two parts. The first part provides the conclusions obtained from the experimental results, and the second part presents the suggestion for the future work.

6.1 Conclusion

6.1.1 Synthesis of graphene oxide and reduced graphene oxide

GO was successfully synthesized by a modified Hummers method, and rGO was prepared from GO via reduction by hydrazine and ammonia.

6.1.2 Varying the amount of rGO in the catalysts

The TiO_2/rGO catalyst was successfully synthesized. The addition of rGO promoted electron transfer and retarded electron-hole recombination. Therefore, the photocatalytic activity of TiO_2/rGO was enhanced. The optimum loading of rGO was 4 %wt in APTMS-TiO_2 (22.1 mmol) and its photocatalytic activity was the highest under both UV and visible light irradiations.

6.1.3 Surface modification of catalyst with varying amount of APTMS

TiO_2/rGO* catalyst was investigated for degradation of methylene blue under UV and visible irradiation. The surface modification of TiO_2 with APTMS 2.21 mmol yielded a higher photocatalytic than the surface modification with APTMS 22.1 mmol. TiO_2/rGO (1:0.04)* catalyst exhibited higher photocatalytic activity than TiO_2/rGO (1:0.04) did because the thin layer of N and Si on TiO_2 surface created the intermediate state within TiO_2 bandgap, resulting in narrower bandgap and slower recombination rate.

6.2 Suggestion

1. Employ another reducing agent or thermal reduction to prepare rGO.

2. Use another coupling agent to modify the surface of TiO_2.

3. Investigate the photodegradation using catalysts in packed bed photoreactor.

REFERENCES

[1]. Dadvar, E., R.R. Kalantary, H. Ahmad Panahi and M. Peyravi, Efficiency of Polymeric Membrane Graphene Oxide-TiO$_2$ for Removal of Azo Dye. *Journal of Chemistry*, 2017, 2017, 1-13.

[2]. Guo, T.-L., J.-G. Li, X. Sun and Y. Sakka, Photocatalytic gro_h of Ag nanocrystals on hydrothermally synthesized multiphasic TiO$_2$ / reduced graphene oxide (rGO) nanocomposites and their SERS performance. *Applied Surface Science*, 2017, 423, 1-12.

[3]. Huangfu, X., Y. Xu, C. Liu, Q. He, J. Ma, C. Ma and R. Huang, A review on the interactions between engineered nanoparticles with extracellular and intracellular polymeric substances from wastewater treatment aggregates. *Chemosphere*, 2019, 219, 766-783.

[4]. Tsang, C.H.A., K. Li, Y. Zeng, W. Zhao, T. Zhang, Y. Zhan, R. Xie, D.Y.C. Leung and H. Huang, Titanium oxide based photocatalytic materials development and their role of in the air pollutants degradation: Overview and forecast. *Environment International*, 2019, 125, 200-228.

[5]. Pu, S., D. Long, Z. Liu, F. Yang and J. Zhu, Preparation of RGO-P25 Nanocomposites for the Photocatalytic Degradation of Ammonia in Livestock Farms. *Catalysts*, 2018, 8(5), 1-14.

[6]. Lai, C., X. Zhou, D. Huang, G. Zeng, M. Cheng, L. Qin, H. Yi, C. Zhang, P. Xu, C. Zhou, R.Z. Wang and C. Huang, A review of titanium dioxide and its highlighted application in molecular imprinting technology in environment. *Journal of the Taiwan Institute of Chemical Engineers*, 2018, 91, 517-531.

[7]. Zhao, Y., Y. Wei, X. Wu, H. Zheng, Z. Zhao, J. Liu and J. Li, Graphene-wrapped Pt/TiO$_2$ photocatalysts with enhanced photogenerated charges separation and reactant adsorption for high selective photoreduction of CO$_2$ to CH$_4$. *Applied Catalysis B: Environmental*, 2018, 226, 360-372.

[8].   Tayel, A., A. Ramadan and O. El Seoud, Titanium Dioxide/Graphene and Titanium Dioxide/Graphene Oxide Nanocomposites: Synthesis, Characterization and Photocatalytic Applications for Water Decontamination. *Catalysts*, 2018, 8(11), 1-45.

[9].   Sun, B., W. Zhou, H. Li, L. Ren, P. Qiao, F. Xiao, L. Wang, B. Jiang and H. Fu, Magnetic Fe_2O_3/mesoporous black TiO2 hollow sphere heterojunctions with wide-spectrum response and magnetic separation. *Applied Catalysis B: Environmental*, 2018, 221, 235-242.

[10].   Ni, Y., W. Wang, W. Huang, C. Lu and Z. Xu, Graphene strongly wrapped TiO_2 for high-reactive photocatalyst: a new sight for significant application of graphene. *Journal of Colloid and Interface Science*, 2014, 428, 162-169.

[11].   Li, J., X. Liu, X. Hou, W. Qin, Z. Sun and L. Pan, Novel reduced graphene oxide wrapped $Bi_{2.38}Mo_{0.81}O_6$ microspheres for highly efficient visible light photocatalysis. *Journal of Colloid and Interface Science*, 2015, 458, 235-240.

[12].   Ye, T., W. Chen, H. Xu, N. Geng and Y. Cai, Preparation of TiO_2/graphene composite with appropriate N-doping ratio for humic acid removal. *Journal of Materials Science*, 2017, 53(1), 613-625.

[13].   Regonini, D., C.R. Bowen, A. Jaroenworaluck and R. Stevens, A review of growth mechanism, structure and crystallinity of anodized TiO_2 nanotubes. *Materials Science and Engineering: R: Reports*, 2013, 74(12), 377-406.

[14].   Fujishima, A. and K. Honda, Electrochemical Photolysis of Water at a Semiconductor Electrode. *Nature Article*, 1972, 238, 37-38.

[15].   Muresan, L.M., Corrosion Protective Coatings for Ti and Ti Alloys Used for Biomedical Implants, in *Intelligent Coatings for Corrosion Control,* 2015, 585-602.

[16].   Larry, L.H. and K.W. Jon, The sol-gel process. *Chemical Reviews*, 1990, 90(1), 33-72.

[17].   Stankovich, S., D.A. Dikin, R.D. Piner, K.A. Kohlhaas, A. Kleinhammes, Y. Jia, Y. Wu, S.T. Nguyen and R.S. Ruoff, Synthesis of graphene-based nanosheets via chemical reduction of exfoliated graphite oxide. *Carbon*, 2007, 45(7), 1558-1565.

[18]. Betancur, A.F., N. Ornelas-Soto, A.M. Garay-Tapia, F.R. Pérez, Á. Salazar and A.G. García, A general strategy for direct synthesis of reduced graphene oxide by chemical exfoliation of graphite. *Materials Chemistry and Physics*, 2018, 218, 51-61.

[19]. Brodie, B., On the atomic Weight of Graphite. *Philosophical Transactions of the Royal Society of London*, 1859, 149, 249-259.

[20]. Staudenmaier, L., Verfahren zur Darstellung der Graphitsäure. *Berichte der deutschen chemischen Gesellschaft*, 1898, 31(2), 1481-1487.

[21]. William S., H., Jr. and O. Richard E., Preparation of Graphitic Oxide. *Journal of the America Chemical Society*, 1958, 80, 1339.

[22]. Moon, I.K., J. Lee, R.S. Ruoff and H. Lee, Reduced graphene oxide by chemical graphitization. *Nature Communications*, 2010, 1, 1-6.

[23]. Lobato, B., V. Vretenar, P. Kotrusz, M. Hulman and T.A. Centeno, Reduced graphite oxide in supercapacitor electrodes. *Journal of Colloid and Interface Science*, 2015, 446, 203-207.

[24]. Li, D., M.B. Muller, S. Gilje, R.B. Kaner and G.G. Wallace, Processable aqueous dispersions of graphene nanosheets. *Nat Nanotechnol*, 2008, 3(2), 101-105.

[25]. De Silva, K.K.H., H.H. Huang, R.K. Joshi and M. Yoshimura, Chemical reduction of graphene oxide using green reductants. *Carbon*, 2017, 119, 190-199.

[26]. Shin, H.-J., K.K. Kim, A. Benayad, S.-M. Yoon, H.K. Park, I.-S. Jung, M.H. Jin, H.-K. Jeong, J.M. Kim, J.-Y. Choi and Y.H. Lee, Efficient Reduction of Graphite Oxide by Sodium Borohydride and Its Effect on Electrical Conductance. *Advanced Functional Materials*, 2009, 19(12), 1987-1992.

[27]. Salehi, M., Z. Shariatinia and A. Sadeghi, Application of RGO/CNT nanocomposite as cathode material in lithium-air battery. *Journal of Electroanalytical Chemistry*, 2019, 832, 165-173.

[28]. Ghasemi, S., S.R. Hosseini and M. Moalem-Banhangi, Preparation of electrochemically reduced graphene oxide/bimetallic copper-platinum nanohybrid as counter electrode for fabrication of dye-sensitized solar cell. *Journal of Electroanalytical Chemistry*, 2019, 833, 242-250.

[29].   Dave, K., N. Pachauri, A. Dinda and P.R. Solanki, RGO modified mediator free paper for electrochemical biosensing platform. *Applied Surface Science*, 2019, 463, 587-595.

[30].   Li, X., S. Zheng, C. Zhang, C. Hu, F. Chen, Y. Sun, S. Duo, R. Zhang, Q. Hu, W. Li and Y. Kang, Synergistic promotion of photocatalytic performance by core@shell structured TiO2/Au@rGO ternary photocatalyst. *Molecular Catalysis*, 2017, 438, 55-65.

[31].   Banerjee, S., P. Benjwal, M. Singh and K.K. Kar, Graphene oxide (rGO)-metal oxide (TiO_2/Fe_3O_4) based nanocomposites for the removal of methylene blue. *Applied Surface Science*, 2018, 439, 560-568.

[32].   Kumar, P., C. Joshi, A. Barras, B. Sieber, A. Addad, L. Boussekey, S. Szunerits, R. Boukherroub and S.L. Jain, Core–shell structured reduced graphene oxide wrapped magnetically separable $rGO@CuZnO@Fe_3O_4$ microspheres as superior photocatalyst for CO_2 reduction under visible light. *Applied Catalysis B: Environmental*, 2017, 205, 654-665.

[33].   Zhang, L., H. Li, Y. Liu, Z. Tian, B. Yang, Z. Sun and S. Yan, Adsorption-photocatalytic degradation of methyl orange over a facile one-step hydrothermally synthesized $TiO_2/ZnO–NH_2–RGO$ nanocomposite. *RSC Advances*, 2014, 4(89), 48703-48711.

[34].   Mohan, V.B., R. Brown, K. Jayaraman and D. Bhattacharyya, Characterisation of reduced graphene oxide: Effects of reduction variables on electrical conductivity. *Materials Science and Engineering: B*, 2015, 193, 49-60.

[35].   Klaysri, R., T. Tubchareon and P. Praserthdam, One-step synthesis of amine-functionalized TiO_2 surface for photocatalytic decolorization under visible light irradiation. *Journal of Industrial and Engineering Chemistry*, 2017, 45, 229-236.

[36].   Hamidipour, L., F. Farzaneh and M. Ghandi, Immobilized $Co(acac)_2$ on modified Fe_3O_4 nanoparticles as a magnetically separable epoxidation catalyst. *Reaction Kinetics, Mechanisms and Catalysis*, 2012, 107(2), 421-433.

[37].   Zhang, Y., L. Song, Y. Zhang, P. Wang, Y. Liu, L. Wu and T. Zhang, A facile method for synthesis of well-coated ZnO@graphene core/shell structure by self-assembly of

amine-functionalized ZnO and graphene oxide. *Chemical Physics Letters*, 2016, 654, 107-113.

[38]. Moorthy, M., A. Govindaraj, B. Madheswaran, B. Kannan and R. Rangappan, Ni(II) incorporated MCM-41 material—heterogeneous catalyst for the C–S and C–N cross coupling reactions. *Journal of Porous Materials*, 2017, 24(5), 1395-1407.

[39]. Adriana, M. and W. L., Methylene blue, an old drug with new indications? *Romanian Journal of Anaesthesia and Intensive Care*, 2010, 17, 35-41.

[40]. Faber, P., A. Ronald and B.W. Millar, Methylthioninium chloride: pharmacology and clinical applications with special emphasis on nitric oxide mediated vasodilatory shock during cardiopulmonary bypass. *Anaesthesia*, 2005, 60, 575-587.

[41]. Ammar, H., L. Hinda, K. Mohamed, E. Elimame, G. Chantal and H. Jean-Marie, Photocatalytic degradation pathway of methylene blue in water. *Applied Catalysis B: Environmental*, 2001, 31, 145-157.

[42]. Iijima, M., S. Takenouchi, I.W. Lenggoro and H. Kamiya, Effect of additive ratio of mixed silane alkoxides on reactivity with TiO_2 nanoparticle surface and their stability in organic solvents. *Advanced Powder Technology*, 2011, 22(5), 663-668.

[43]. Fadillah, G., S. Wahyuningsih and A.H. Ramelan, Enhanced Photovoltaic Performance by Surface Modification of TiO_2 Nanorods with Aminopropyltrimethoxysilane (APTMS). *IOP Conference Series: Earth and Environmental Science*, 2017, 75, 1-6.

[44]. Kominami, H., M. Itonaga, A. Shinonaga, K. Kagawa, S. Konishi and Y. Kera, Preparation of vanadium-based catalysts for selective catalytic reduction of nitrogen oxides using titania supports chemically modified with organosilanes, in *Scientific Bases for the Preparation of Heterogeneous Catalysts - Proceedings of the* 8*th International Symposium, Louvain-la-Neuve, Belgium* 9-12, 2002, 1089-1096.

[45]. Zhao, J., M. Milanova, M.M.C.G. Warmoeskerken and V. Dutschk, Surface modification of TiO_2 nanoparticles with silane coupling agents. *Colloids and Surfaces A: Physicochemical and Engineering Aspects*, 2012, 413, 273-279.

[46]. Pasqui, D. and R. Barbucci, Synthesis, characterization and self cleaning properties of titania nanoparticles grafted on polyester fabrics. *Journal of Photochemistry and Photobiology A: Chemistry*, 2014, 274, 1-6.

[47]. Sun, H., S. Liu, S. Liu and S. Wang, A comparative study of reduced graphene oxide modified TiO_2, ZnO and Ta_2O_5 in visible light photocatalytic/photochemical oxidation of methylene blue. *Applied Catalysis B: Environmental*, 2014, 146, 162-168.

[48]. Zou, L., X. Wang, X. Xu and H. Wang, Reduced graphene oxide wrapped CdS composites with enhanced photocatalytic performance and high stability. *Ceramics International*, 2016, 42(1), 372-378.

[49]. Amaranatha Reddy, D., R. Ma, M.Y. Choi and T.K. Kim, Reduced graphene oxide wrapped $ZnS–Ag_2S$ ternary composites synthesized via hydrothermal method: Applications in photocatalyst degradation of organic pollutants. *Applied Surface Science*, 2015, 324, 725-735.

[50]. Sirisuk, A., H.J. Charles G. and A. Marc A., Photocatalytic degradation of ethylene over thin films of titania supported on glass rings. *Catalysis Today*, 1999, 54, 159-164.

[51]. Petro, R., P. Borodulin, T.E. Schlesinger and M. Schlesinger, Liquid Exfoliated Graphene: A Practical Method for Increasing Loading and Producing Thin Films. *ECS Journal of Solid State Science and Technology*, 2015, 5(2), 36-40.

[52]. Xu, T., L. Zhang, H. Cheng and Y. Zhu, Significantly enhanced photocatalytic performance of ZnO via graphene hybridization and the mechanism study. *Applied Catalysis B: Environmental*, 2011, 101(3-4), 382-387.

[53]. Alexander, L. and H.P. Klug, Determination of Crystallite Size with the X‑Ray Spectrometer. *Journal of Applied Physics*, 1950, 21(2), 137-142.

[54]. Sun, Z., J. Guo, S. Zhu, J. Ma, Y. Liao and D. Zhang, High photocatalytic performance by engineering Bi_2WO_6 nanoneedles onto graphene sheets. *RSC Advances*, 2014, 4(53), 27963-27970.

[55]. Setiadji, S., B.W. Nuryadin, H. Ramadhan, C.D.D. Sundari, T. Sudiarti, A. Supriadin and A.L. Ivansyah, Preparation of reduced Graphene Oxide (rGO) assisted by

microwave irradiation and hydrothermal for reduction methods. *IOP Conference Series: Materials Science and Engineering*, 2018, 434, 1-8.

[56]. Cheshme, K., H. Amir, G. Moussavi and A.R. Mahjoub, The preparation of TiO_2@rGO nanocomposite efficiently activated with UVA/LED and H_2O_2 for high rate oxidation of acetaminophen: Catalyst characterization and acetaminophen degradation and mineralization. *Applied Surface Science*, 2018, 440, 963-973.

[57]. Biris, A.R., D. Toloman, A. Popa, M.D. Lazar, G.K. Kannarpady, V. Saini, F. Watanabe, B.P. Chhetri, A. Ghosh and A.S. Biris, Synthesis of tunable core–shell nanostructures based on TiO_2-graphene architectures and their application in the photodegradation of rhodamine dyes. *Physica E: Low-dimensional Systems and Nanostructures*, 2016, 81, 326-333.

[58]. Wei, Q., Y. Wang, H. Qin, J. Wu, Y. Lu, H. Chi, F. Yang, B. Zhou, H. Yu and J. Liu, Construction of rGO wrapping octahedral Ag-Cu_2O heterostructure for enhanced visible light photocatalytic activity. *Applied Catalysis B: Environmental*, 2018, 227, 132-144.

[59]. Sharma, A. and B.K. Lee, Rapid photo-degradation of 2-chlorophenol under visible light irradiation using cobalt oxide-loaded TiO_2 / reduced graphene oxide nanocomposite from aqueous media. *Journal of Environmental Economics and Management*, 2016, 165, 1-10.

[60]. Chong, S.W., C.W. Lai and S.B. Abdul Hamid, Green preparation of reduced graphene oxide using a natural reducing agent. *Ceramics International*, 2015, 41(8), 9505-9513.

[61]. Sengar, P., G.A. Hirata, M.H. Farias and F. Castillón, Morphological optimization and (3-aminopropyl) trimethoxy silane surface modification of $Y_3Al_5O_{12}$:Pr nanoscintillator for biomedical applications. *Materials Research Bulletin*, 2016, 77, 236-242.

[62]. Zhang, J., H. Song, Y. Chen, T. Hao, F. Li, D. Yuan, X. Wang, L. Zhao and J. Gao, Amino-modified molecular sieves for adsorptive removal of H_2S from natural gas. *RSC Advances*, 2018, 8(66), 38124-38130.

[63]. Vilvamani, N., R.D. Gupta and S.K. Awasthi, Ru(ii)–polypyridyl complex-grafted silica nanohybrids: versatile hybrid materials for Raman spectroscopy and photocatalysis. *RSC Advances*, 2015, 5(18), 13451-13461.

[64]. Avcioglu, G.S., B. Ficicilar, A. Bayrakceken and I. Eroglu, High performance PEM fuel cell catalyst layers with hydrophobic channels. *International Journal of Hydrogen Energy*, 2015, 40(24), 7720-7731.

[65]. Douda, J., C.R. González Vargas, E.V. Basiuk, A.I. Díaz Cano, J.A. Fuentes García and X.A. Hernández Contreras, Optical properties of amine-functionalized graphene oxide. *Applied Nanoscience*, 2019, 9(4), 567-578.

[66]. Irie, H., Y. Watanabe and K. Hashimoto, Nitrogen-Concentration Dependence on Photocatalytic Activity of $TiO_{2-x}N_x$ Powders. *The Journal of Physical Chemistry B*, 2003, 107(23), 5483-5486.

[67]. Yang, G., Z. Jiang, H. Shi, T. Xiao and Z. Yan, Preparation of highly visible-light active N-doped TiO_2 photocatalyst. *Journal of Materials Chemistry*, 2010, 20(25), 5301-5309.

[68]. Xiao, J., Z. Pan, B. Zhang, G. Liu, H. Zhang, X. Song, G. Hu, C. Xiao, Z. Wei and Y. Zheng, The research of photocatalytic activity on Si doped TiO_2 nanotubes. *Materials Letters*, 2017, 188, 66-68.

[69]. Asahi, R., T. Morikawa, T. Ohwaki, K. Aoki and Y. Taga, Visible-Light Photocatalysis in Nitrogen-Doped Titanium Oxides. *Science*, 2001, 293(5528), 269-271.

[70]. Abazari, R., A.R. Mahjoub and G. Salehi, Preparation of amine functionalized g-C_3N_4@(H/S)MOF NCs with visible light photocatalytic characteristic for 4-nitrophenol degradation from aqueous solution. *Journal of Hazardous Materials*, 2019, 365, 921-931.

[71]. Li, K., F. Lu, R. Fan, C. Ma and B. Xu, Effect of Er local surrounding on photoluminescence of Si Er co-doped ZnO film. *Journal of Luminescence*, 2018, 200, 9-13.

[72]. Lin, Z., K. Chen, P. Zhang, J. Xu, H. Dong, W. Li, Y. Ji and X. Huang, The Role of N-Si-O Defect States in Optical Gain from an a-SiN_xO_y/SiO_2 Waveguide and in Light Emission from an n-a-SiN_xO_y/p-Si Heterojunction LED. *physica status solidi (a)*, 2018, 215(12), 1-7.

[73]. Bao, N., G. Wu, J. Niu, Q. Zhang, S. He and J. Wang, Wide spectral response and enhanced photocatalytic activity of TiO_2 continuous fibers modified with aminosilane coupling agents. *Journal of Alloys and Compounds*, 2014, 599, 40-48.

[74]. Yan, M.F. and W.W. Rhodes, Low Temperature Sintering of TiO_2. *Materials Science and Engineering: B*, 1983, 61, 59-66.

APPENDICES

APPENDIX A

CALIBRATION CURVE OF METHYLENE BLUE

The calibration curve of methylene blue used for calculation concentration of methylene blue in photodegradation of methylene blue. The concentration of methylene blue was investigated at 0, 0.5, 2, 4, 6, 8, 10, and 12, respectively (shown in Figure 33).
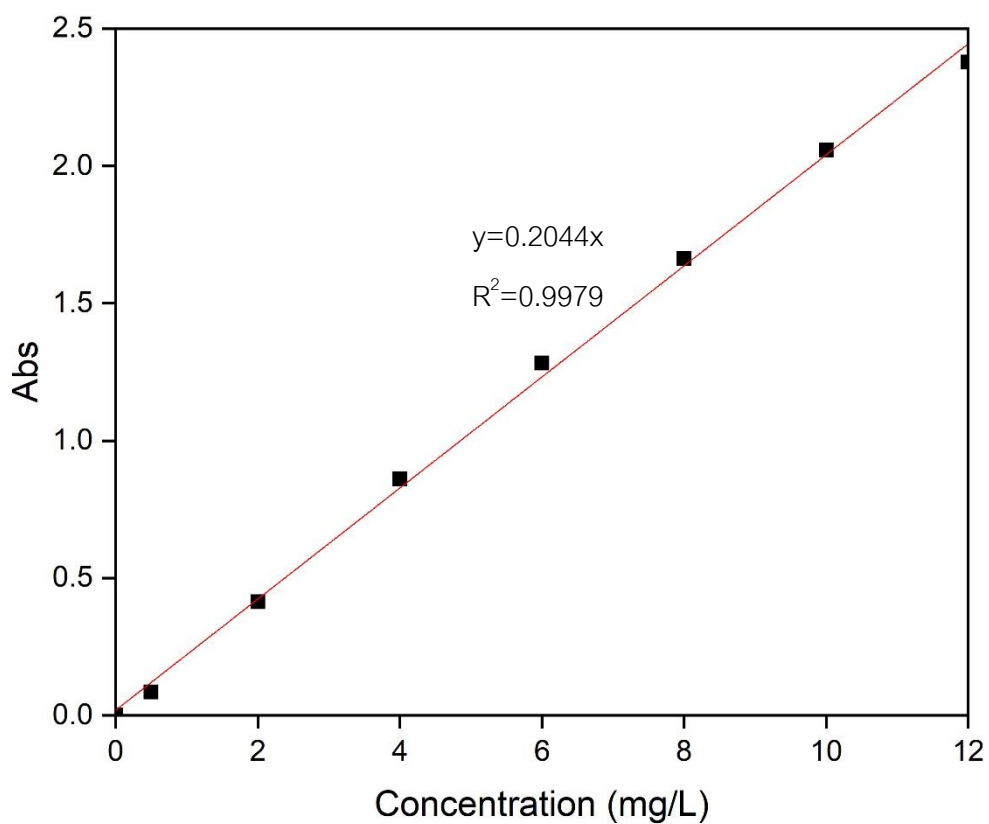
Figure 33 The calibration curve of methylene blue from UV-vis spectrophotometer

(Perkin-Elmer lambda 650)

APPENDIX B

LIGHTING INSTRUMENT

Both UV and visible bulbs were used as a light source in methylene blue degradation reaction. Measure the intensity of light by the light sensor (IL 1700 research radiometer), as shown in the Table 15

Table 15 properties of the light blub

Type of light	Brand	Power (W)	Wavelength (nm)	Intensity by sensor UV light (%)	Intensity by sensor visible light (%)
UVC light	Philip	75	200-280	99.69	0.31
Visible light (Daylight)	Philip	18	400-700	1.01	98.99

APPENDIX B

THE PHOTOCATALYTIC REACTOR DESIGNED

FOR METHYLENE BLUE DEGRADATION

Cabinet was designed for use in photocatalytic reactions, cabinet is 400 cm wide, 400 cm long and 1000 cm high. The cabinet can be opened in 2 positions: the top for collecting methylene blue solution and the front for set up the experimental. The inside of the cabinet was attached to the aluminium foil sheet to reflect light. The slat was drilled to allow the wires to be placed outside. The two 200 V fan was installed on the right side of cabinets for cooling (as seen in Figure 34).
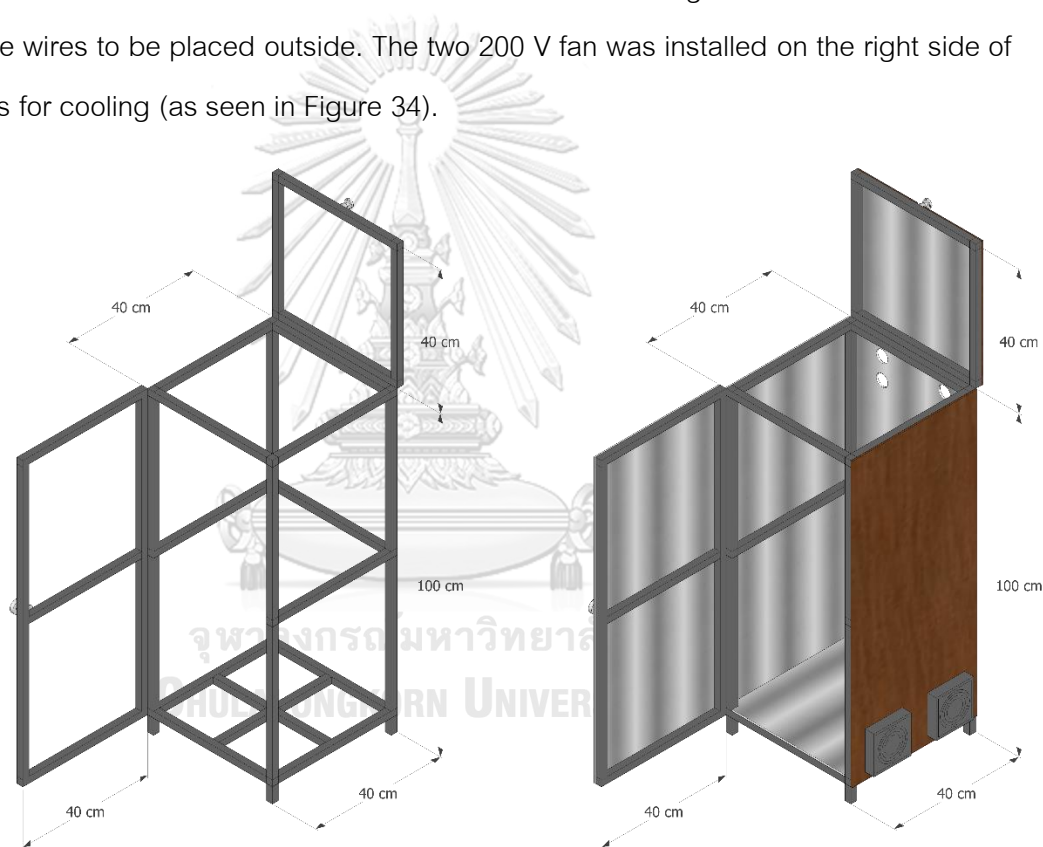

Figure 34 Cabinet design

Double jacketed reactor was designed for use in photocatalytic reactions, it is a double layer of glass cylinder. The inner cylinder has a radius of 3 cm, 32 cm high and the outer cylinder has a radius of 6 cm, 30 cm high. The space between the bottom of the inner cylinder and the outer cylinder is 1.5 cm (as seen in Figure 35).

The inner cylinder was designed to fit the light bulb. The outer cylinder was designed to contain methylene blue solution. The pipes connected to the outer cylinder, designed to pour methylene blue. The space between the inner cylinder and outer cylinder was designed to insert a magnetic bar.
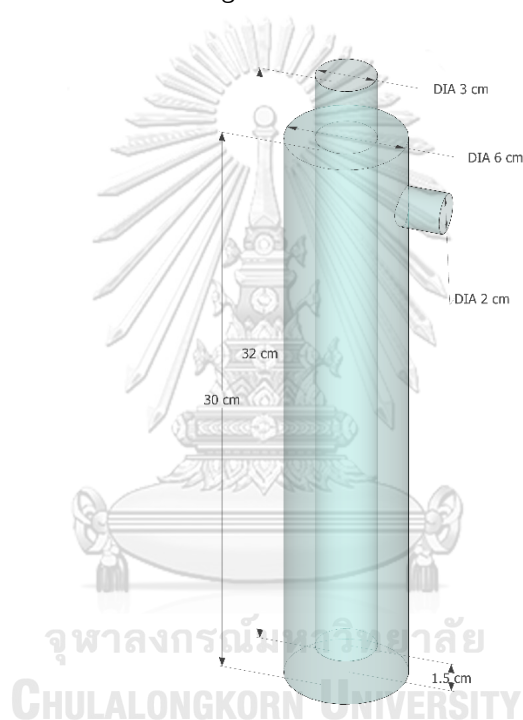

Figure 35 Double jacketed reactor design

APPENDIX D

CALCULATION OF THE CRYSTALLITE SIZE

The crystallite size of TiO_2 was calculated by combining the Debye-Scherer equation (Equations (10)) and Warren formula (Equations (11) to (12))

Debye-Scherer equation:

$$D = \frac{k\lambda}{\beta cos\theta} \tag{10}$$

Where

D = Crystallite size (Å)

k = Crystallite-shape factor (0.9)

λ = X-ray wavelength (1.5418 Å for CuK$_\alpha$)

β = X-ray diffraction broadening (radian)

θ = Observed peak angel (degree)

The X-ray diffraction broadening (β) can be obtained by using the Warren formula.

Warren formula:

$$\beta^2 = \beta_M^2 - \beta_S^2 \tag{11}$$

$$\beta = \sqrt{\beta_M^2 - \beta_S^2} \tag{12}$$

Where

β_M = Measured peak width in radians at half peak height

β_S = Corresponding width of a standard material

Example: Calculation of the crystallite site of pure TiO_2 calcined at 400 °C for 2 hours

   Finding the half-weight width (101) diffraction peak at 25.4° from the XRD pattern

The half-weight width (101) diffraction peak = 1.06°

$$= \frac{2\pi \times 1.06}{360}$$

$$= 0.0185 \text{ radian}$$

The corresponding half-height width of peak of **α**-alumina = 0.0038 radian

The broading

$$\beta = \sqrt{\beta_M^2 - \beta_S^2}$$

$$= \sqrt{0.0185^2 - 0.0038^2}$$

$$\beta = 0.0181 \text{ radian}$$

$$2\theta = 25.4°$$

$$\theta = 12.7°$$

$$\lambda = 1.54 \text{ Å}$$

The crystallite size

$$D = \frac{k\lambda}{\beta \cos\theta}$$

$$= \frac{(0.9)(1.54)}{(0.0181)\cos(12.7)}$$

$$= 77.26 \text{ Å} \qquad = 7.73 \text{ nm}$$

APPENDIX E

CALCULATION OF WEIGHT FRACTION OF ANATASE, RUTILE AND BROOKITE PHASE OF TiO_2

Finding 2θ of TiO_2 can be found from the XRD pattern (as seen in Figure 36), which can divide 2θ into each phase as shown in the Table 16.

The weight fraction of TiO_2 can be calculated (shown in Equations (13) to (15) below).

$$W_A = \frac{k_A A_A}{k_A A_A + A_R + k_B A_B} \tag{13}$$

$$W_R = \frac{A_R}{k_A A_A + A_R + k_B A_B} \tag{14}$$

$$W_B = \frac{k_B A_B}{k_A A_A + A_R + k_B A_B} \tag{15}$$

Where

W_A	=	Weight fraction of anatase phase
W_R	=	Weight fraction of rutile phase
W_B	=	Weight fraction of brookite phase
A_A	=	The intensity of the anatase peak
A_R	=	The intensity of the rutile peak
A_B	=	The intensity of the brookite peak
k_A	=	The coefficient factor of anatase (0.886)
k_B	=	The coefficient factor of brookite (2.721)

Example: Calculation of the phase contents of pure TiO_2 calcined at 400 °C for 2 hours
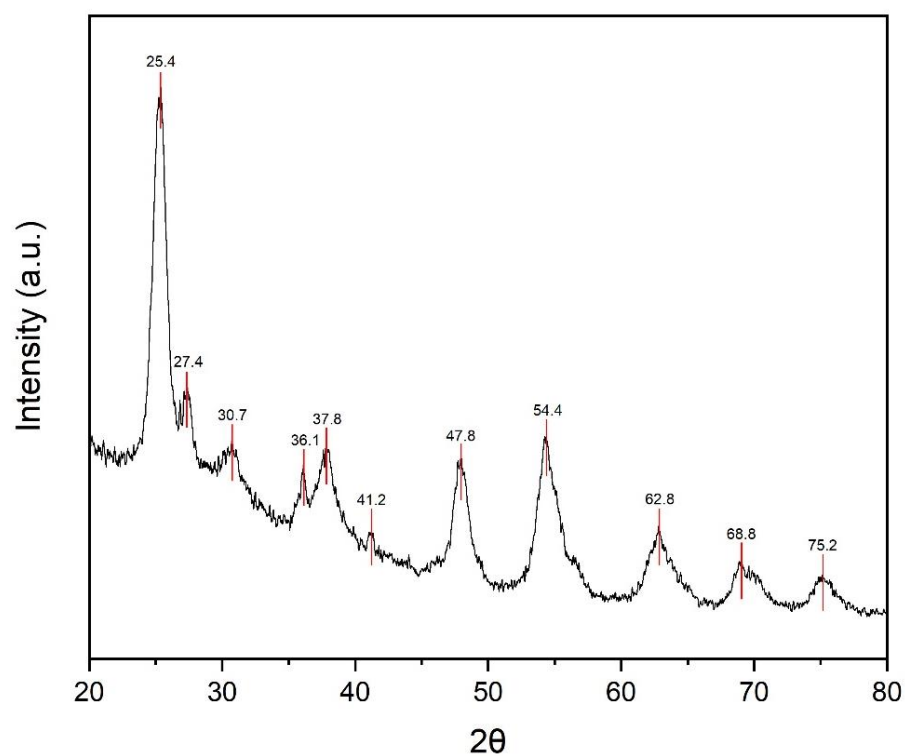
Figure 36 XRD pattern of pure TiO_2 calcined at 400 °C for 2 hours

Table 16 The 2θ peak of TiO_2 phase by XRD

Phase	2θ
Anatase	25.4
	37.8
	47.8
	54.4
	68.8
	75.2
Rutile	27.4
	36.1
	41.2
	62.8
Brookite	30.7

Calculation of the intensity using the OriginLab program at 2θ of 25.4, 27.4, and 30.7 were integrated the intensity as follows: 821.12, 27.38, and 88.98 respectively.

$$W_A = \frac{(0.886)(1721.038)}{(0.886)(821.12)+(27.38)+(2.271)(88.98)} = 0.72$$

$$W_R = \frac{(355.6781)}{(0.886)(821.12)+(27.38)+(2.271)(88.98)} = 0.17$$

$$W_B = \frac{(2.271)(88.9822)}{(0.886)(25.4)+(27.38)+(2.271)(88.98)} = 0.11$$

จุฬาลงกรณ์มหาวิทยาลัย

CHULALONGKORN UNIVERSITY

APPENDIX F

THE CALCULATION OF THE BANDGAP FROM UV-VIS SPECTRA

From UV-vis spectra can be used to calculate the bandgap of semiconductor material by plotting $(\alpha h \nu)^{\frac{1}{n}}$ versus photon energy (hν). The photon energy (hν) and optical absorption coefficient (α) were estimated by equation (16)-(17)

$$h\nu = E_g = \frac{hc}{\lambda} \tag{16}$$

$$h\nu = \frac{1240}{\lambda} \tag{17}$$

Where

E_g	=	Bandgap of catalyst (eV)
h	=	Plank constant (6.62×10^{-34} Joules·sec)
c	=	Speed of light (3.0×10^{8} meter/sec)
λ	=	Wavelength from UV-vis spectra (nm)

Note: 1 eV is 1.6×10^{-19} Joules

$$\alpha = \frac{2.303A}{t} \tag{16}$$

Where

α	=	Optical absorption coefficient
A	=	Absorbance
t	=	Thickness of the sample

Example: Calculation of the bandgap of TiO_2

From $(\alpha h\nu)^{\frac{1}{n}}$, the power factor (n) is 0.5 because this graph finds direct bandgap.

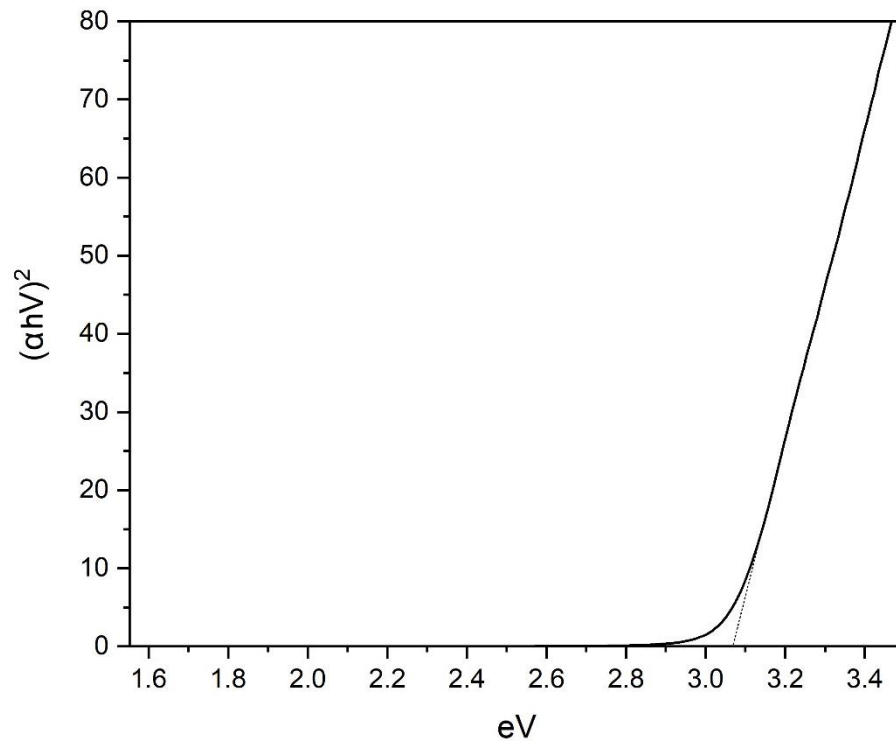**Figure 37** The bandgap of TiO_2

From Figure 37, A line cut the X axis presented the bandgap is 3.06 eV.

VITA

NAME	Sirinya Kanjanapanasont
DATE OF BIRTH	25 November 1994
PLACE OF BIRTH	Bangkok
INSTITUTIONS ATTENDED	Graduated high school from Triamudomsuksapattanakarn Ratchada school in 2013.
	Graduated Bachelor's Degree faculty of Applied Science in Industrial Chemistry, King Mongkut's University of Technology North Bangkok, Thailand in 2017.
HOME ADDRESS	327-329 Soi inthamara 55, Sutthisan road, Dindaeng Sub-district, Dindaeng District, Bangkok, 10400
PUBLICATION	Sirinya Kanjanapanasont and Akawat sirisuk. Application of amine-functionalized TiO_2 wrapped in reduced graphene oxide wrapped in photocatalytic degradation of methylene blue. Proceeding of pure and applied chemistry International conference, Mahidol University, Bitec, Bangkok, Thailand. Feb. 7-8, 2019 (PACCON 2019)

จุฬาลงกรณ์มหาวิทยาลัย
CHULALONGKORN UNIVERSITY